Conducting Metal Dithiolene Complexes: Structural and Electronic Properties

Reizo Kato

Condensed Molecular Materials Laboratory, RIKEN (The Institute of Physical and Chemical Research), 2-1 Hirosawa, Wako-shi, Saitama 351-0198, Japan

Received March 9, 2004

Contents

Reizo Kato was born in 1955 in Yamaguchi, Japan. He received his B.Sc. in 1979, M.Sc. in 1981, and D.Sc. in 1984 from the University of Tokyo. He was appointed research associate of Department of Chemistry at Toho University in 1984, and he was promoted to lecturer in 1988. He joined the Institute for Solid State Physics in The University of Tokyo as an associate professor in 1990. Since 1999 he has been a chief scientist and a director of the Condensed Molecular Materials laboratory in RIKEN (The Institute of Physical and Chemical Research). He received the Chemical Society of Japan Award for Young Chemists in 1990 and the IBM Japan Science Prize in 1995 for his works on molecular conductors. His research has been focused on development of new molecular materials, especially molecular metals and superconductors.

1. Introduction: History and Background

Since the first report of superconductivity in synthetic organic conductors in 1980, chemistry and physics of molecular-based conductors have achieved remarkable progress and a number of exotic phenomena have been reported. From the viewpoint of the electronic structure, this progress has been driven along the following two major trends: (1) from "one-dimensional" to "higher dimensional" and (2) from "single-component" to "multicomponent".[1]

Since planar π-conjugated molecules tend to stack to form the column structure, molecular metals developed in the early stage had the one-dimensional (1D) electronic structure. The 1D metallic electron system characterized by a pair of planar Fermi surface is inherently unstable and undergoes a metal−insulator transition accompanied by the density wave formation at low temperatures.[2] Much effort to increase the dimensionality of the electronic structure has been made by means of chemical modification and/or application of pressure. The first organic superconducting system, $(TMTSF)_2X$ (TMTSF = tetramethyltetraselenafulvalene), forms a quasi-1D system.[3] The organic donor BEDT-TTF (ET, bis(ethylenedithio)tetrathiafulvalene) has provided various types of two-dimensional (2D) metallic systems.[4] And, the DCNQI-Cu (DCNQI = *N*,*N*′-dicyanoquinonediimine) salt is the first molecular conductor where the existence of a three-dimensional (3D) Fermi surface is confirmed.[5] On the other hand, for many years, molecular conductors were assumed to be electronically single-component systems which exhibit only one electron type. Although the first organic metal TTF-TCNQ (TTF = tetrathiafulvalene; TCNQ = tetracyanoquinodimethane) is well-known to consist of two conducting components, the electronic structure of this system has an only 1D pπ electron character.[1] Over the past decade, however, an increasing number of multicomponent systems, where there exist "two" energy bands with different characters (for example, orbital character and dimensionality) near the Fermi level or where a strong interaction between itinerant pπ electrons and localized d electron spins operates, have been reported.

10.1021/cr030655t CCC: $48.50
Published on Web 08/27/2004

Scheme 1

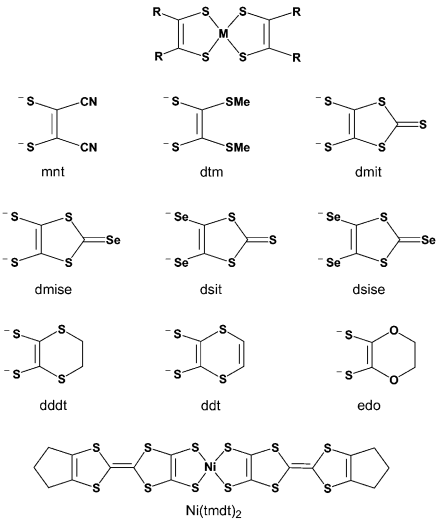

These systems exhibit exotic physical properties derived from an interplay of various components. The DCNQI-Cu system where pπ electrons coexist with itinerant d electrons is a typical example.[5] In this review, since the interplay of different types of energy bands is mainly discussed, the multicomponent would be interpreted as "multiband".

In terms of the band theory, the metallic state is due to the formation of at least one partially filled energy band (in other words, the system has a Fermi surface). A straightforward application of this concept in the molecular system can be achieved by arranging open-shell molecules (radicals) so as to enable intermolecular electron transfer. In most cases, cation radicals or anion radicals generated by the chemical or electrochemical method have been used for the formation of metallic molecular crystals. It should be noted that this is not the only approach to the molecular metal, as one can see, for example, in the single-component molecular metal (vide infra). Metal bis-1,2-dithiolene complexes, as well as organic donors and acceptors, have been intensively studied as the component of molecular conductors and have provided a unique category of conducting materials.[6] This review focuses almost entirely on the Ni, Pd, Pt, and Au complexes with the square-planar coordination geometry. Dithiolene ligands are known to stabilize unusual oxidation states. Metal dithiolene complexes possess a delocalized electron system as a planar central core $M(C_2S_2)_2$ and exist as a series of compounds in different formal oxidation states with the same central metal ion. Depending on the choice of substituent groups (R in Scheme 1) attached to the central core, metal dithiolene complexes behave as both the donor and the acceptor. Table 1 shows an example of the tuning of electrochemical properties by the choice of dithiolene ligands, where the potentials E_1 and E_2 are correlated to the donor (acceptor) ability and the ΔE ($=E_1 - E_2$) value can be a measure of the on-site Coulomb energy.[7] Electrochemical data suggest that the acceptor (donor) ability and the on-site Coulomb energy for each mixed-ligand complex are intermediate between those of the corresponding symmetrical complexes, respectively.

Table 1. Electrochemical Data for [Ni(X)(Y)] Salts

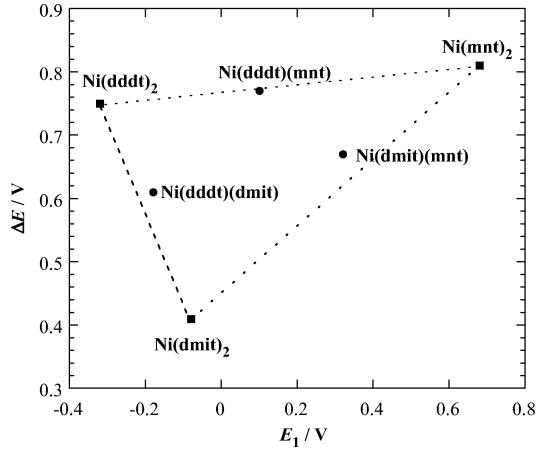

TBA[Ni(X)(Y)][a]	E_1[b]/V (0 ↔ −1)	E_2[c]/V (−1 ↔ −2)	ΔE[d]/V
TBA[Ni(dddt)$_2$]	−0.32	−1.07	0.75
TBA[Ni(dmit)$_2$]	−0.08	−0.49	0.41
TBA[Ni(mnt)$_2$]	+0.68	−0.13	0.81
TBA[Ni(dmit)(dddt)]	−0.18	−0.79	0.61
TBA[Ni(dddt)(mnt)]	+0.10	−0.67	0.77
TBA[Ni(dmit)(mnt)]	+0.32	−0.35	0.67

[a] TBA = $(n\text{-}C_4H_9)_4N$. [b] Irreversible. [c] Reversible. [d] $\Delta E = E_1 - E_2$. Measured at a Pt electrode in CH_3CN, 0.1 M TBAP (volts vs 0.01 M $Ag/AgNO_3$). Temperature, 25 °C. Dotted lines in the figure are guides for the eyes.

Concerning molecular conductors based on metal complexes, partially oxidized tetracyanoplatinate salts (for example, KCP = $K_2[Pt(CN)_4]Br_{0.30}\cdot 3H_2O$) and related materials were intensively studied in the first stage.[8] In these highly conducting salts, the square-planar platinum complexes are stacked to form a linear Pt-atom chain with a very short Pt⋯Pt distance (2.8−3.0 Å). The metallic state in these salts originates from a partially filled energy band associated with the overlap of $5dz^2$ orbitals of the central platinum atoms along the stack. The first observation of metallic behavior in the metal dithiolene complexes was reported for $(H_3O)_{0.33}Li_{0.8}[Pt(mnt)_2]\cdot 1.67H_2O$ (mnt = maleonitriledithiolate) in 1981.[9] The Pt⋯Pt distance (3.639 Å) in this salt is much larger than those in the KCP type conductors, which indicates that the conduction pathway cannot be formed by the overlapping of the $5dz^2$ orbitals. On the other hand, the LUMO of the neutral $Pt(mnt)_2$ molecule has dominantly ligand character and the direct overlapping of the planar complexes with the interplanar distance of 3.592 Å enables the intermolecular electron transfer through the ligand π orbitals. Therefore, the conduction band is formed by the ligand π orbitals or mixed-metal−ligand orbitals where the sulfur atoms play an important role, which indicates a resemblance to a situation in conducting cation radical salts derived from TTF type organic donor molecules. This illustrated the new aspect of the molecular conductors based on the metal complexes.

In 1983, the first conducting $M(dmit)_2$ salt (dmit = 1,3-dithiole-2-thione-4,5-dithiolate), $(Bu_4N)_2[Ni(dmit)_2]_7\cdot 2CH_3CN$, was reported.[10] In terms of molecular architecture where the central electron-delocalized core is extended by the sulfur-containing

Table 2. Molecular Superconductors Based Metal Dithiolene Complexes

compound	T_c/K	P/kbar	ref
(TTF)[Ni(dmit)$_2$]$_2$	1.62	7	12
α-(EDT-TTF)[Ni(dmit)$_2$]	1.3		14
(Me$_4$N)[Ni(dmit)$_2$]$_2$	5	7	13
α′-(TTF)[Pd(dmit)$_2$]$_2$	5.93	24	15
α-(TTF)[Pd(dmit)$_2$]$_2$	1.7	22	16
β-(Me$_4$N)[Pd(dmit)$_2$]$_2$	6.2	6.5	17
(Et$_2$Me$_2$N)[Pd(dmit)$_2$]$_2$	4	2.4	18
β′-(Et$_2$Me$_2$P)[Pd(dmit)$_2$]$_2$	4	6.9	19
β′-(Me$_4$Sb)[Pd(dmit)$_2$]$_2$	3	10	20
β′-(Me$_4$As)[Pd(dmit)$_2$]$_2$	4	7 ($\|\|b$)	21

heterorings, the M(dmit)$_2$ molecule is similar to the organic donor BEDT-TTF. In the crystal, the planar Ni(dmit)$_2$ molecules are stacked and short S···S distances are observed between molecules in different stacks. This indicates that the isotrithione rings incorporated into the dithiolene moiety can enhance the transverse S···S contacts. Many of the Ni(dmit)$_2$-based molecular conductors, however, are revealed to have a 1D electronic structure, which is due to the symmetry of the frontier orbital as discussed in section 2. A genuine 2D electronic structure based on the Ni(dmit)$_2$ molecule was first found in α-(Et$_2$-Me$_2$N)[Ni(dmit)$_2$]$_2$, which exhibits the new type of molecular arrangement "spanning overlap".[11] In 1986, (TTF)[Ni(dmit)$_2$]$_2$ was reported to undergo a superconducting transition at 1.62 K under 7 kbar.[12] This is the first report of the superconductor based on the metal dithiolene complex. The superconductivity in the system where the electron conduction originates from only the M(dmit)$_2$ molecule was first found in (Me$_4$N)[Ni(dmit)$_2$]$_2$ at 5 K under 7 kbar.[13] Up to now, ten M(dmit)$_2$ compounds including one ambient-pressure superconductor have been reported to exhibit the superconductivity (Table 2).

The concept of "two-band systems" for the M(dmit)$_2$ compounds proposed in 1989 gave an essential impact to the study of the electronic structure of molecular conductors based on the metal dithiolene complexes.[22] The small HOMO−LUMO (HOMO = highest occupied molecular orbital; LUMO = lowest unoccupied molecular orbital) level splitting in the M(dmit)$_2$ molecule leads to an interplay of two different types of energy bands associated with the HOMO and LUMO around the Fermi level, which means that some M(dmit)$_2$ compounds can belong to the multicomponent system. This picture can be available to other metal dithiolene complexes. When the M(dmit)$_2$ molecules are strongly dimerized in the crystal, the small HOMO−LUMO level splitting induces a HOMO−LUMO band inversion and provides 2D electronic structures associated with the HOMO-based energy band. A typical example is the β(β′) type Pd(dmit)$_2$ system.[23]

The metal instability accompanied by the density wave formation in the 1D system (Peierls instability) has been overcome by the effort to increase the dimensionality of the electronic structure. Yet, there exist other mechanisms that lead to the insulating state. Among them, the strong electron−electron correlation is rather general and plays an important role.[24] In systems with a half-filled energy band, where each unit in the crystal has one conduction electron, strong on-site Coulomb interaction induces the Mott-insulating state if the conduction band is narrow. It should be noted that the Mott insulating state can occur even in the 2D or 3D system. Many molecular conductors belong to the (effectively) half-filled band system with the narrow bandwidth (W) and the strong on-site Coulomb repulsion (U). The β(β′) type Pd(dmit)$_2$ system is also the Mott insulator at ambient pressure. The Mott insulator can turn metallic, when the bandwidth is enhanced (correctly, the correlation parameter U/W is reduced) or the half-filled state is removed by the doping of holes or electrons. An important point is that the superconducting phase is frequently situated between the metallic phase and the Mott insulating phase, as is the case for the high-T_c oxides.[24] The application of pressure can effectively enhance the bandwidth as well as the dimensionality of the electronic structure. The pressure effect on the β(β′) type Pd(dmit)$_2$ system has been investigated in terms of the strong correlation.

In the Mott insulating state, spin degrees of freedom play a crucial role in determining physical properties. In the Mott insulator where the total number of (conduction) electrons is equal to the total number of lattice sites, electrons are localized at each site to avoid the on-site Coulomb repulsion. Such a situation quite often results in a magnetically ordered state, for example, an antiferromagnetic ordered state. In geometrically frustrated spin systems, however, a long-range ordering of spins is suppressed by the existence of a large number of minimal energy spin configurations. Among them, antiferromagnets with a triangular lattice have attracted extensive interest.[25] In 2002, it was reported that the temperature dependence of the magnetic susceptibilities of the β(β′) type Pd(dmit)$_2$ salts was explained by the model of the spin-$^1/_2$ Heisenberg triangular antiferromagnet.[26] This is the first time this was reported in molecular systems and indicates that the spin frustration operates in this system. The competition between the spin frustration and the antiferromagnetic ordering in the Mott insulators is an important subject. Theoretical studies of ground states in strongly correlated molecular conductors including the system with an approximately triangular lattice structure have been systematically performed.[27] It is suggested that the spin frustration can diminish the stability of the insulating state by destroying the antiferromagnetic correlation and induce the paramagnetic metal state.[28]

Cooperative electronic materials where itinerant π electrons interact with localized spins are categorized to another type of multicomponent system, and much effort has been aimed toward the preparation of this class of materials. Cation radical salts of the organic donor perylene with anionic M(mnt)$_2$ species (M = Ni, Pd, Pt, Cu, Au) were studied in terms of coupled electronic and magnetic transitions in 1D systems.[29] In these compounds, the M(mnt)$_2$ complexes form localized spin systems and do not form the conduction band.

Table 3. Molecular Conductors Based on M(mnt)$_2$

compound	conducting behavior at ambient pressure [pressure effect][a]	properties of crystal and electronic structures	ref
α-(perylene)$_2$[Ni(mnt)$_2$]	T_{M-I} = 25 K, $\sigma_{RT} \sim 700$ S cm^{-1}	segregated regular stacking arrangement	31
β-(perylene)$_2$[Ni(mnt)$_2$]	shallow resistivity minimum around 250−260 K, σ_{RT} = 50−90 S cm^{-1}, E_a = 0.090 eV at 100 K	disordered structure	31
(perilo[1,12-*b*,*c*,*d*]thiophene)$_3$-[Ni(mnt)$_2$]$_2$	S, $\sigma_{RT} \sim 9$ S cm^{-1}, E_a = 0.168 eV	segregated stacking arrangement dimerization	32
(DT-TTF)$_2$[Ni(mnt)$_2$]	T_{M-I} = 120 K, σ_{RT} = 40 S cm^{-1}	segregated regular stacking arrangement	33
(BEDT-TTF)[Ni(mnt)$_2$]	−	no S···S contacts between donor and acceptor	34
(EDO-TTFI$_2$)$_2$[Ni(mnt)$_2$]	T_{M-I} = 88 K, σ_{RT} = 110 S cm^{-1}	segregated 1D stacking arrangement ferromagnetic interaction between cation and anion	35
(perylene)$_2$[Pd(mnt)$_2$]	T_{M-I} = 28 K, σ_{RT} = 250−300 S cm^{-1}	segregated regular stacking arrangement	36
(ITTF)$_2$[Pd(mnt)$_2$]	$\sigma_{RT} = 2 \times 10^{-6}$ S cm^{-1} (pellet)	mixed stack structure	37
Cs$_{0.83}$[Pd(mnt)$_2$]·0.5H$_2$O	S, σ_{RT} = 5 S cm^{-1} [M (>1.4 K) at 13 kbar]	eclipsed dimer pair 2D interdimer S···S contacts	38
(H$_3$O)$_{0.33}$Li$_{0.8}$[Pt(mnt)$_2$]·1.67H$_2$O	T_{M-I} = 220 K, $\sigma_{RT} \sim 200$ S cm^{-1}	1D regular stacking arrangement with an eclipsed configuration 1D system	39
Li$_{0.5}$[Pt(mnt)$_2$]·2H$_2$O	S, σ_{RT} = 1 S cm^{-1}, small anisotropy within the (001) plane	fourfold stacking arrangement	40
Rb[Pt(mnt)$_2$]·2H$_2$O	S, $\sigma_{RT} = 2.5 \times 10^{-5}$ S cm^{-1}, E_a = 0.240 eV (<250 K), 0.300 eV (>250 K)	1D dimerized stacking arrangement	41
(perylene)$_2$[Pt(mnt)$_2$]	T_{M-I} = 6.5 K, σ_{RT} = 500−600 S cm^{-1} [increase of T_{M-I} with pressure]	segregated regular stacking arrangement	36
(DT-TTF)$_2$[Pt(mnt)$_2$]	T_{M-I} = 127 K, σ_{RT} = 40 S cm^{-1}	segregated regular stacking arrangement	42
(EDO-TTFI$_2$)$_2$[Pt(mnt)$_2$]	T_{M-I} = 96 K, σ_{RT} = 170 S cm^{-1}	segregated 1D stacking arrangement ferromagnetic interaction between cation and anion	35
(perylene)$_2$[Au(mnt)$_2$]	broad resistivity minimum at 50−60 K, σ_{RT} = 500−600 S cm^{-1} [an anomaly in the derivative of the resistivity at 24 K (>17 kbar)]	segregated regular stacking arrangement	36
(BET-TTF)[Au(mnt)$_2$]	S, $\sigma_{RT} = 8 \times 10^{-3}$ S cm^{-1}, E_a = 0.090 eV	mixed stack structure	43
(DT-TTF)$_2$[Au(mnt)$_2$]	broad resistivity minimum around 220 K, σ_{RT} = 9 S cm^{-1}	segregated regular stacking arrangement dimerization of donor molecules (<220 K) two-leg spin-ladder configuration	42
(BDNT)[Au(mnt)$_2$]$_2$	S, $\sigma_{RT} = 1 \times 10^{-7}$ S cm^{-1}, E_a = 0.19 eV	crisscross stacks dimerization	44
(perylene)$_2$[Fe(mnt)$_2$]	T_{M-I} = 58 K, σ_{RT} = 200 S cm^{-1}	segregated 1D stacking arrangement dimerization	45
(perylene)$_2$[Co(mnt)$_2$]	T_{M-I} = 73 K, σ_{RT} = 200 S cm^{-1}		45
(perylene)[Co(mnt)$_2$]·0.5CH$_2$Cl$_2$	T_{M-S} = 277 K, T_{S-S} = 170−190 K, σ_{RT} = 60 S cm^{-1}	segregated stacking arrangement S···Co contacts dimerized polymer of Co(mnt)$_2$ 1D system disorder of solvent molecules	46
(perylene)$_4$[Co(mnt)$_2$]$_3$		trimerization with S···Co contacts alternate packing of perylene and Co(mnt)$_2$ trimer units	47

[a] M = metallic, S = semiconducting, I = insulating, SC = superconducting.

In the course of the development of molecular conductors, it has been revealed that their electronic states are quite sensitive to molecular arrangement and orientation. The molecular packing in the crystal is determined by the total balance of many weak intermolecular interactions, including van der Waals interaction, hydrogen bonding, and $\pi-\pi$ interaction. Design of the intermolecular interaction is indispensable in the rational development of the molecular conductors to still higher forms. An introduction of supramolecular chemistry is a possible solution to this subject.[30] In the case of molecular conductors based on the metal dithiolene complexes, several attempts to introduce the supramolecular cation effect have been reported.[6h,30]

This review deals with some selected topics concerning crystal and electronic structures of the conducting metal dithiolene complexes, including M(mnt)$_2$ (Table 3), M(dmit)$_2$ (Table 4), Se-analogues of M(dmit)$_2$ (Table 5), M(dddt)$_2$ (dddt = 5,6-dihydro-1,4-dithiin-2,3-dithiolate; Table 6), and Ni(edo)$_2$ (edo = 5,6-dihydro-1,4-dioxin-2,3-dithiolate) derivatives (Table 7) from the viewpoint of chemical and physical control of conducting properties in the molecular conductors (molecular structures of components are shown in Schemes 1 and 2). Most of this review will be devoted to the M(dmit)$_2$ compounds because they have been investigated most intensively and have enjoyed increasing use in the design and preparation of new conducting molecular materials. It should be added that several leading reviews[6] have focused on other topics including preparation and magnetic properties, and readers are referred to these works for these topics.

2. Molecular Orbital Aspect: HOMO–LUMO Interplay

The molecular conductors often have simple and clear electronic structures which can be approximately described by the simple tight-binding band calculation. In most molecular metals, the conduction

Table 4. Molecular Conductors Based on M(dmit)$_2$

compound	conducting behavior at ambient pressure [pressure effect][a]	properties of crystal and electronic structures	ref
(TTF)[Ni(dmit)$_2$]$_2$	M, σ_{RT} = 300 S cm^{-1} [SC, T_{SC} = 1.62 K at 7 kbar]	segregated 1D stacking arrangement parallel band multisheet Fermi surface	12, 48
(DBTTF)[Ni(dmit)$_2$]	σ_{RT} = 300 S cm^{-1}	segregated 1D stacking arrangement parallel band	49
α-(EDT-TTF)[Ni(dmit)$_2$]	SC, T_{SC} = 1.3 K	solid crossing column structure	14, 50
β-(EDT-TTF)[Ni(dmit)$_2$]	S, σ_{RT} = 0.01 S cm^{-1}	mixed stack structure	50a
γ-(EDT-TTF)[Ni(dmit)$_2$]	T_{M-I} = 100 K	parallel column structure	50b
(BEDT-TTF)[Ni(dmit)$_2$]	S, σ_{RT} = 2 × 10^{-3} S cm^{-1}	segregated uniform side-by-side array	51
α-(BPDT-TTF)[Ni(dmit)$_2$]	T_{S-I} = 120 K, σ_{RT} = 5−10 S cm^{-1}	segregated 1D stacking arrangement narrow energy gap	52
(TMTSF)[Ni(dmit)$_2$]	S, σ_{RT} = 300 S cm^{-1}, E_a ∼ 0.034 eV	segregated 1D stacking arrangement	53
(OMTSF)[Ni(dmit)$_2$]	S, σ_{RT} ∼ 1S cm^{-1}, E_a = 0.12 eV	mixed stack	54
α-(BPDT-TSeF)[Ni(dmit)$_2$]$_2$	T_{M-I} ∼ 130 K	segregated regular stacking arrangement	55
β-(BPDT-TSeF)[Ni(dmit)$_2$]$_2$	I	dimerization	55
(BPDT-TSeF)[Ni(dmit)$_2$]	T_{M-I} = 162 K, σ_{RT} = 100 S cm^{-1}	uniform 1D side-by-side array	55, 56
[Pt(dddt)$_2$][Ni(dmit)$_2$]$_2$	σ_{RT} = 5 × 10^{-5} S cm^{-1} (powder)	Ni(dmit)$_2$ stacks perpendicular to Pt(dddt)$_2$ entities	57
(NH$_2$Me$_2$)[Ni(dmit)$_2$]$_2$	S, σ_{RT} = 0.1S cm^{-1}, E_a = 0.21 eV	weakly dimerized stacking cation disorder	58
(NHMe$_3$)[Ni(dmit)$_2$]$_2$	T_{M-I} = 220 K, σ_{RT} = 140 S cm^{-1} [decrease of the conductivity with increasing pressure]	weakly dimerized stacking cation disorder quasi-1D system	58
(NHMe$_3$)$_2$[Ni(dmit)$_2$]$_5$·2CH$_3$CN	S, σ_{RT} = 0.2S cm^{-1}, E_a = 0.23 eV	stacking of monomers and weak dimers	58
(NH$_3$Me)$_2$[Ni(dmit)$_2$]$_5$·2CH$_3$CN	S, σ_{RT} = 1.5 S cm^{-1}, E_a = 0.20 eV	stacking of monomers and weak dimers cation disorder	58
(Me$_4$N)[Ni(dmit)$_2$]$_2$	T_{M-I} ∼ 100 K [SC, T_{SC} = 5.0 K at 7 kbar]	solid crossing column structure weakly dimerized stacking	13, 59
α-(Et$_2$Me$_2$N)[Ni(dmit)$_2$]$_2$	M (>0.5 K), σ_{RT} = 20−100 S cm^{-1} resistivity jump at 240−245 K	spanning overlap 2D system with quasi-3D interaction	10, 60
β-(Et$_2$Me$_2$N)[Ni(dmit)$_2$]$_2$	S, σ_{RT} = 3 S cm^{-1}	strongly dimerized stacking cation disorder	61
γ-(Et$_2$Me$_2$N)[Ni(dmit)$_2$]$_2$	M (>2 K) no resistivity jump	spanning overlap	62
(EtMe$_3$N)[Ni(dmit)$_2$]$_2$	S, σ_{RT} = 0.4 S cm^{-1}	strongly dimerized stacking cation disorder	61
(Et$_4$N)[Ni(dmit)$_2$]$_2$	S, σ_{RT} = 4.5 × 10^{-2} S cm^{-1}, E_a = 0.16 eV	weakly dimerized stacking	63
(Bu$_4$N)$_2$[Ni(dmit)$_2$]$_7$·2CH$_3$CN	S, σ_{RT} = 1 S cm^{-1}, E_a = 0.042 eV	interstack S···S contacts	9, 64, 68b
(*N*,*N*-dimethylpyrrolidinium)-[Ni(dmit)$_2$]$_2$	S	strongly dimerized stacking	65
(*N*,*N*-dimethylpiperidinium)-[Ni(dmit)$_2$]$_2$	M (>0.5 K)	spanning overlap	65, 66
(Me$_4$P)[Ni(dmit)$_2$]$_2$	S, σ_{RT} = 0.6 S cm^{-1}	κ-like arrangement	61
(MePh$_3$P)[Ni(dmit)$_2$]$_3$	S, σ_{RT} = 0.1 S cm^{-1}, E_a = 0.22 eV	dimer-based packing	67
(Ph$_4$P)[Ni(dmit)$_2$]$_3$	S, σ_{RT} = 7 S cm^{-1}, E_a = 0.010 eV (<100 K), 0.017 eV (>100 K)	dimerized stacking + monomer	68
(benzyltriphenylphosphonium)-[Ni(dmit)$_2$]$_3$	S, σ_{RT} = 0.2 S cm^{-1}	threefold stacking	57b
(Me$_4$As)[Ni(dmit)$_2$]$_2$	S, σ_{RT} = 0.1 S cm^{-1}	dimer-based packing	61
(Ph$_4$As)$_{0.25}$[Ni(dmit)$_2$]	S, σ_{RT} = 10−15 S cm^{-1}, E_a = 0.010 eV (<150 K), 0.030 eV (>150 K)	solid crossing column structure	69
(Me$_3$S)[Ni(dmit)$_2$]$_2$	S, σ_{RT} = 6.5 × 10^{-2} S cm^{-1}, E_a = 0.13 eV	twofold stacking	61, 57b, 68b
(Me$_3$SO)[Ni(dmit)$_2$]$_2$	S, σ_{RT} = 1 S cm^{-1}	tetramer-based packing	61
(Me$_3$Te)[Ni(dmit)$_2$]$_2$	T_{M-I} = 65 K	solid crossing column structure S···Te interaction less 1D character	70
(Me$_3$Te)[Ni(dmit)$_2$]$_3$·(CH$_3$)$_2$CO	S, σ_{RT} = 0.25 S cm^{-1}	herringbone arrangement	70
α-(MeTeC$_4$H$_8$O)[Ni(dmit)$_2$]$_2$	T_{M-I} = 170 K, σ_{RT} = 2.5 S cm^{-1}	almost uniform 1D stacking S···Te interaction multisheet Fermi surface	70
β-(MeTeC$_4$H$_8$O)[Ni(dmit)$_2$]$_2$	temperature-independent σ (> ∼50 K), σ_{RT} = 10 S cm^{-1}	herringbone arrangement S···Te and O···Te interactions multisheet Fermi surface	70
γ-(MeTeC$_4$H$_8$O)[Ni(dmit)$_2$]$_2$	S, σ_{RT} = 0.17 S cm^{-1}	fourfold stacking S···Te interaction	70
(acridinium)[Ni(dmit)$_2$]$_3$	M (>0.4 K), σ_{RT} = 45 S cm^{-1} [no SC at 8 and 13 kbar (>0.4 K)]	spanning overlap	71
(phenazinium)[Ni(dmit)$_2$]$_3$	S, σ_{RT} = 4 S cm^{-1}, E_a = 0.11 eV	weakly dimerized stacking 2D network of S···S contacts	71b
[(2-methoxyethyl)ammonium]-[Ni(dmit)$_2$]$_3$·CH$_3$CN		threefold stacking hydrogen bond (−NH$^+$···S=)	72
(morpholinium)$_2$[Ni(dmit)$_2$]$_3$	S, σ_{RT} = 0.1 S cm^{-1}, E_a = 0.10 eV	1D columnar structure hydrogen bond (−NH$^+$···S=)	72
(*N*-methylmorpholinium)-[Ni(dmit)$_2$]$_2$	S, σ_{RT} = 4 S cm^{-1}, E_a = 0.10 eV	fourfold stacking hydrogen bond (−NH$^+$···S=)	72

Table 4 (Continued)

compound	conducting behavior at ambient pressure [pressure effect][a]	properties of crystal and electronic structures	ref
(1,2,3-trimethylimidazolium)-[Ni(dmit)$_2$]	S, σ_{RT} = 0.21 S cm^{-1}, E_a = 0.11 eV	possible quasi-3D anion network cation disorder	73
(guanidinium)[Ni(dmit)$_2$]$_2$	S, σ_{RT} = 32 S cm^{-1}, E_a = 0.12 eV	1D and 2D networks of S···S contacts hydrogen bond	74
(1,1-dimethylguanidinium)-[Ni(dmit)$_2$]$_2$	S, σ_{RT} = 0.15 S cm^{-1}, E_a = 0.13 eV	2D network of S···S contacts hydrogen bond	74
[Me$_3$N(CH$_2$)$_4$NMe$_3$][Ni(dmit)$_2$]$_5$·2DMF	S, σ_{RT} = 0.1−1 S cm^{-1}, E_a ~ 0.19 eV	stacking of monomers and dimers	75
[Me$_3$N(CH$_2$)$_4$NMe$_3$][Ni(dmit)$_2$]$_5$·2CH$_3$CN	S, σ_{RT} = 1−0.1 S cm^{-1}, E_a ~ 0.20 eV	alternate stacking of dimers, and trimers	75
Li$_2$(12-crown-4)$_3$[Ni(dmit)$_2$]$_7$·2(CH$_3$)$_2$CO	T_{S-S} = 250 K, σ_{RT} = 30 S cm^{-1} [no deviation from an Arrhenius plot at 10.2 kbar]	stacking of trimers and monomers	76
Li$_{0.6}$(15-crown-5)[Ni(dmit)$_2$]$_2$·H$_2$O	M around RT, σ_{RT} ~ 240 S cm^{-1}	1D ion channel structure uniform 1D column	77
(NH$_4$)(15-crown-5)$_2$[Ni(dmit)$_2$]	I	dimerization	76a
(NH$_4$)(18-crown-6)[Ni(dmit)$_2$]$_3$	S, σ_{RT} = 0.4 S cm^{-1}	weakly timerized stacking	76a
(*p*-EYPNN)[Ni(dmit)$_2$]	S, σ_{RT} = 1.3 × 10^{-4} S cm^{-1}, E_a = 0.27 eV ($\|\|c$)	1D ladder chain	78
[4-(dimethylamino)-1-methyl-pyridinium][Ni(dmit)$_2$]	S, σ_{RT} = 1.3 × 10^{-2} S cm^{-1}, E_a = 0.05 eV	2D S···S contacts	79
α(α′)-(TTF)[Pd(dmit)$_2$]$_2$	σ_{RT} = 750 S cm^{-1}	segregated regular stacking arrangement	15, 16, 48b, 80
	T_{M-I} = 220 K (α, irreversible; α′, reversible)	parallel band	
	[SC, T_{SC} = 1.7 K at 22 kbar (α)]	multisheet Fermi surface	
	T_{SC} = 5.93 K at 24 kbar (α′)	α(RT) → *β*(low temp) → *γ*(RT) phase transition induced by heat cycle	
δ-(TTF)[Pd(dmit)$_2$]$_2$	T_{M-I} = 120 K, σ_{RT} = 100 S cm^{-1}	dimerization	80
α′-(EDT-TTF)[Pd(dmit)$_2$]	T_{M-M} = 50 K, σ_{RT} = 58 S cm^{-1} [suppression of the 50 K anomaly above 5 kbar]	solid crossing column structure dimerization	81
(EDT-TTF)$_2$[Pd(dmit)$_2$]$_3$	σ_{RT} = 120 S cm^{-1}	trimerization semiconductive band structure	81a
γ-(EDT-TTF)[Pd(dmit)$_2$]	M (>100 K, $\|\|(a+c)$), σ_{RT} = 100 S cm^{-1} [shift of the M−I transition down to the low-temperature region under pressure (<12.2 kbar)]	parallel column structure dimerization 2D system	50b
(IEDT)[Pd(dmit)$_2$]	T_{M-M} = 80 K	parallel column structure dimerization S···I interaction quasi-2D system	82
α-(Me$_4$N)[Pd(dmit)$_2$]$_2$	S, σ_{RT} = 50 S cm^{-1} [T_{M-I} ~ 60 K (>6 kbar)]	solid crossing column structure dimerization	83
β-(Me$_4$N)[Pd(dmit)$_2$]$_2$	S, σ_{RT} = 50 S cm^{-1} [SC, T_{SC} = 6.2 K at 6.5 kbar]	solid crossing column structure dimerization 2D system	17, 83, 84
β′-(Me$_4$P)[Pd(dmit)$_2$]$_2$	S, σ_{RT} ~ 50 S cm^{-1} [T_{M-I} = 30−40 K at 13.2 kbar]	solid crossing column structure dimerization quasi-triangular lattice 2D system	85
β′-(Me$_4$As)[Pd(dmit)$_2$]$_2$	S, σ_{RT} ~ 1 S cm^{-1} [SC, T_{SC} = 4 K at 7 kbar ($\|\|b$)]	solid crossing column structure dimerization quasi-triangular lattice 2D system	21, 83, 85b
β′-(Me$_4$Sb)[Pd(dmit)$_2$]$_2$	S, σ_{RT} ~ 10 S cm^{-1} [SC, T_{SC} = 3 K at 10 kbar]	solid crossing column structure dimerization quasi-triangular lattice 2D system	20a, 85b,c
(Et$_2$Me$_2$N)[Pd(dmit)$_2$]$_2$	S, σ_{RT} = 10−80 S cm^{-1} [SC, T_{SC} = 4 K at 2.4 kbar]	single column dimerization	18
β′-(Et$_2$Me$_2$P)[Pd(dmit)$_2$]$_2$	S, σ_{RT} ~ 10 S cm^{-1} [SC, T_{SC} = 4 K at 6.9 kbar]	solid crossing column structure dimerization quasi-triangular lattice 2D system	19, 85c, 86
β′-(Et$_2$Me$_2$As)[Pd(dmit)$_2$]$_2$	S, σ_{RT} ~ 30 S cm^{-1} [M (>1.5 K) at 16.1 kbar]	solid crossing column structure dimerization quasi-triangular lattice 2D system	20a, 86
β′-(Et$_2$Me$_2$Sb)[Pd(dmit)$_2$]$_2$	S, σ_{RT} ~ 1 S cm^{-1} [M (>1.5 K) at 16.4 kbar]	solid crossing column structure dimerization quasi-triangular lattice 2D system	20a, 85c, 86
(Et$_4$N)$_{0.5}$[Pd(dmit)$_2$]	S, σ_{RT} = 0.7 S cm^{-1}, E_a = 0.10 eV	dimerization	87
(*n*-Bu$_4$N)$_{0.5}$[Pd(dmit)$_2$]	T_{M-I} = 240 K, σ_{RT} = 12 S cm^{-1}	dimerization cation disorder	88

Table 4 (Continued)

compound	conducting behavior at ambient pressure [pressure effect][a]	properties of crystal and electronic structures	ref
$(n\text{-}Bu_4N)_{0.33}[Pd(dmit)_2]$	$T_{M-I} = 120$ K (upon cooling), $\sigma_{RT} = 150$ S cm^{-1}	dimerization cation disorder	88
$(Me_3S)[Pd(dmit)_2]_2$	S [small σ change (> ~150 K), σ_{RT} = 100 S cm^{-1} at 9.9 kbar] [enhancement of the insulating behavior at 16.1 kbar]	parallel column structure dimerization 2D system	89
$(EtMe_2S)[Pd(dmit)_2]_2$	S [M (> ~100 K) above 5.5 kbar]	single column dimerization 2D system	89
$(Et_2MeS)[Pd(dmit)_2]_2$	small σ change (>150 K), $\sigma_{RT} = 100$ S cm^{-1} [shift of the M−I transition down to the low-temperature region under pressure]	parallel column structure dimerization	57b, 90
$(Et_2MeS)_{0.5}[Pd(dmit)_2]$	S, $\sigma_{RT} = 10-40$ S cm^{-1}, $E_a \sim 0.06$ eV	dimerization cation disorder	90
$(Me_3Te)[Pd(dmit)_2]_2$	M (>50 K)	solid crossing column structure S···Te interaction dimerization	91
$(Et_2MeTe)[Pd(dmit)_2]_2$	M (>30−40 K)	parallel column structure S···Te interaction	91, 92
(quinuclidinium)$[Pd(dmit)_2]_2$	$T_{M-M} \sim 200$ K $T_{M-I} \sim 40$ K [suppression of the 200 K anomaly at 12 kbar]	solid crossing column structure	93
$Cs[Pd(dmit)_2]_2$	$T_{M-I} = 56.5$ K	solid crossing column structure dimerization	94
$(TTF)[Pt(dmit)_2]_3$	S, $\sigma_{RT} = 20$ S cm^{-1}	alternate stacking of dimers and monomers	48a
$(HMTTeF)_2[Pt(dmit)_2]$	S, $\sigma_{RT} = 20$ S cm^{-1}	HMTTeF tetramer	95
$(Me_4N)[Pt(dmit)_2]_2$	small σ change (>220 K), $\sigma_{RT} \sim 10$ S cm^{-1} [enhancement of nonmetallic behavior under pressure]	solid crossing column structure dimerization	96
$(NHMe_3)[Pt(dmit)_2]_3{\cdot}CH_3CN$	almost constant σ (>180 K) $\sigma_{RT} = 140$ S cm^{-1}	dimerization interstack S···S contacts	58
$(Me_4N)[Au(dmit)_2]_2$	S, $\sigma_{RT} = 5-15$ S cm^{-1}	solid crossing column structure	97
$\beta\text{-}(Et_4N)[Au(dmit)_2]_2$	S, $\sigma_{RT} = 1.0$ S cm^{-1}	isostructural with $(Et_4N)[Ni(dmit)_2]_2$	98
$(Et_4N)[Au(dmit)_2TCNQ]$	I	mixed stack	98, 99
$(BEDT\text{-}TTF)_3[V(dmit)_3]_2$	S, $\sigma_{RT} = 3$ S cm^{-1}, $E_a = 0.025$ eV	1D system	100

[a] M = metallic, S = semiconducting, I = insulating, SC = superconducting.

Table 5. Molecular Conductors Based on Se-Analogues of M(dmit)$_2$

compound	conducting behavior at ambient pressure [pressure effect][a]	properties of crystal and electronic structures	ref
(EDT-TTF)$[Ni(dmise)_2]$	$T_{M-I} = 100$ K, $\sigma_{RT} = 100$ S cm^{-1}	segregated regular stacks parallel column structure	101
$(NH_3Me)[Ni(dmise)_2]_2$	S, $\sigma_{RT} = 4.5$ S cm^{-1}, $E_a = 0.072$ eV	herringbone arrangement	102
$(NH_2Me_2)[Ni(dmise)_2]_2$	almost constant σ (>100 K), $\sigma_{RT} = 30$ S cm^{-1}	quasi-3D interaction	102
$(NHMe_3)[Ni(dmise)_2]_2$	M (around RT), $\sigma_{RT} = 100$ S cm^{-1} [M (>60 K) at 6 kbar]	3D system	101, 102
$\alpha\text{-}(Me_4N)[Ni(dmise)_2]_2$	small σ change (>140 K), $\sigma_{RT} \sim 1$ S cm^{-1}	κ-like arrangement	103
$\beta\text{-}(Me_4N)[Ni(dmise)_2]_2$	S, $\sigma_{RT} = 10$ S cm^{-1}, $E_a = 0.05$ eV	solid crossing column structure dimerization	103
(*N*,*N*-dimethylpiperidinium)$[Ni(dmise)_2]_2$	M (>2 K), $\sigma_{RT} = 70$ S cm^{-1}	spanning overlap	104
$(Me_4P)[Pd(dmise)_2]_2$	S, $\sigma_{RT} \sim 100$ S cm^{-1} [almost constant σ (>4.2 K) at 20 kbar]	solid crossing column structure dimerization 2D system	85b
$(Me_4As)[Pd(dmise)_2]_2$	S, $\sigma_{RT} \sim 100$ S cm^{-1} [M (>4.2 K) at 13.2 kbar] [nonmetallic at 16.3 kbar]	solid crossing column structure dimerization 2D system	85b
$(Me_4Sb)[Pd(dmise)_2]_2$	S, $\sigma_{RT} \sim 100$ S cm^{-1} [M (>60 K) at 6.1 kbar] [nonmetallic at 15 kbar]	solid crossing column structure dimerization 2D system	85b
$(Me_4N)[Ni(dsise)_2]_2$	S, $\sigma_{RT} = 12$ S cm^{-1}, $E_a = 0.06$ eV	dimerization with Se···Ni contacts	105
$\beta\text{-}(Me_4N)[Pd(dsit)_2]_2$	almost constant σ (>220 K), $\sigma_{RT} = 30-70$ S cm^{-1} [$T_{M-I} = 70$ K at 10.7 kbar]	solid crossing column structure dimerization with Pd···Pd contact	85a

[a] M = metallic, S = semiconducting, I = insulating, SC = superconducting.

band originates from only one frontier molecular orbital (HOMO for donor or LUMO for acceptor) which is calculated for the isolated molecule by the extended Hückel molecular orbital (MO) method. This is because the intermolecular transfer energy among frontier molecular orbitals is smaller than the energy differences among molecular orbitals. This single-MO picture enabled quasi-quantitative analy-

Table 6. Molecular Conductors Based on M(dddt)$_2$

compound	conducting behavior at ambient pressure[a]	properties of crystal and electronic structures	ref
[Ni(dddt)$_2$]$_3$(HSO$_4$)$_2$	T_{M-I} = 25 K	2D semimetal	106
[Ni(dddt)$_2$]$_3$(BF$_4$)$_2$	S, σ_{RT} = 1 S cm^{-1}	weak trimerization different charge states	107
[Ni(dddt)$_2$]$_3$(ClO$_4$)$_2$	S, σ_{RT} = 0.25 S cm^{-1}	strong trimerization with S···Ni contacts	108
[Ni(dddt)$_2$]$_3$(AuBr$_2$)$_2$	M (>1.3 K)	side-by-side S···S contacts	109
[Pd(dddt)$_2$]Ag$_{1.54}$Br$_{3.50}$	M (>4.2 K)	uniform stacking arrangement 2D system	110
[Pd(dddt)$_2$]$_2$AuBr$_2$	S, σ_{RT} = 2.0 S cm^{-1}	dimerization	111
[Pd(dddt)$_2$]$_2$IBr$_2$	S, σ_{RT} = 0.5−1.0 S cm^{-1}	dimerization	111
[Pd(dddt)$_2$]$_2$GaBr$_4$	S, σ_{RT} = 0.25 S cm^{-1}, E_a = 0.66 eV	dimerization 2D S···S contacts	112
[Pd(dddt)$_2$]$_2$CF$_3$SO$_3$	S, σ_{RT} = 1 S cm^{-1}	dimerization	113
[Pt(dddt)$_2$]$_2$IBr$_2$	S, σ_{RT} = 5−10 S cm^{-1}	dimerization	107b
[Pt(dddt)$_2$]$_2$ICl$_2$	S, σ_{RT} = 5−10 S cm^{-1}	dimerization	107b
[Pt(dddt)$_2$]$_2$AuBr$_2$	S, σ_{RT} = 0.5−1.0 S cm^{-1}	dimerization	107b
[Pt(dddt)$_2$]$_3$(BF$_4$)$_2$	σ_{RT} = 0.5−1.0 S cm^{-1}	isostructural with (ET)$_3$X$_2$ (X = BF$_4$, ClO$_4$)	107b
[Pt(dddt)$_2$]$_2$FeCl$_4$	S, σ_{RT} = 1−0.06 S cm^{-1}	isostructural with [Pt(dddt)$_2$]$_2$GaBr$_4$	114

[a] M = metallic, S = semiconducting, I = insulating, SC = superconducting.

Table 7. Molecular Conductors Based on Ni(edo)$_2$ and Its Mixed-ligand Derivatives

compound	conducting behavior at ambient pressure[a]	properties of crystal and electronic structures	ref
[Ni(edo)$_2$]$_3$(PF$_6$)$_2$	S, σ_{RT} = 9.1 × 10^{-5}, E_a = 0.2 eV	trimer-based κ type packing spanning overlap	115
[Ni(edo)$_2$]$_2$FeCl$_4$	I	trimerization charge separation	115
[Ni(edo)$_2$]$_2$FeBr$_4$	I	twisted stack	115
[Ni(ddt)(edo)]$_2$BF$_4$	S, σ_{RT} = 5.6 × 10^{-3}, E_a = 0.2 eV	head-to-head stacking	115
[Ni(dddt)(edo)]$_3$(FeCl$_4$)$_2$	S, σ_{RT} = 1.0 × 10^{-4}, E_a = 0.5 eV	twisted donor arrangement 1D system	115
[Ni(dtm)(edo)]$_2$ClO$_4$	S, σ_{RT} = 7.7× 10^{-5}, E_a = 0.4 eV	fourfold stack 1D system	115

[a] M = metallic, S = semiconducting, I = insulating, SC = superconducting.

Scheme 2

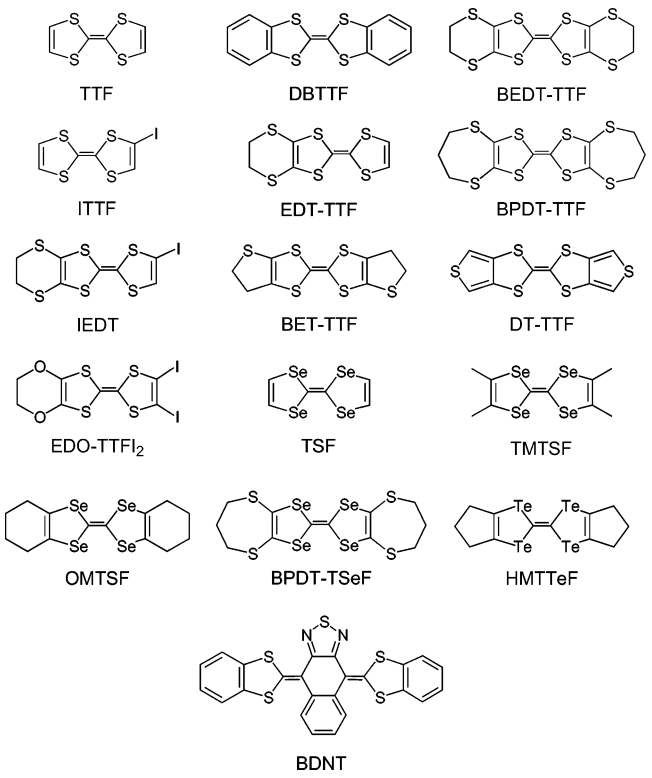

sis of the electronic structure using only overlap integrals derived from the crystal structure data and opened a way to the molecular design especially for the construction of the higher dimensional electronic

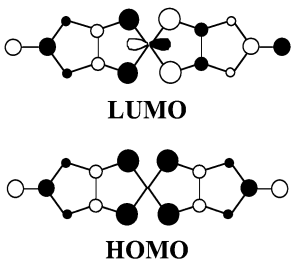

Figure 1. HOMO and LUMO of M(dmit)$_2$.

system. On the other hand, if the HOMO−LUMO energy splitting is comparable to the intermolecular transfer integrals, two types of energy bands should be located near the Fermi level. Such a two-MO picture was first pointed out for (TTF)[Ni(dmit)$_2$]$_2$ and α′-(TTF)[Pd(dmit)$_2$]$_2$.[22]

Figure 1 shows the HOMO and LUMO of an ideal M(dmit)$_2$ molecule with D_{2h} symmetry. They are different in symmetry; b_{2g} for the LUMO and b_{1u} for the HOMO. Although the metal d_{xz} orbital can mix into the LUMO, the HOMO has no contribution from the metal d orbitals due to its symmetry. Consequently, there is no metal−ligand interaction which stabilizes the HOMO and the HOMO−LUMO energy splitting Δ is reduced in the M(dmit)$_2$ molecule. Despite its importance in the band structure, the Δ value is difficult to estimate exactly. The extended Hückel MO calculation for the M(dmit)$_2$ molecule using a single-ζ basis set for the nonmetal atoms and a double-ζ basis set for transition metal atoms indicates that Δ is about 0.4 eV.[6e] On the other hand,

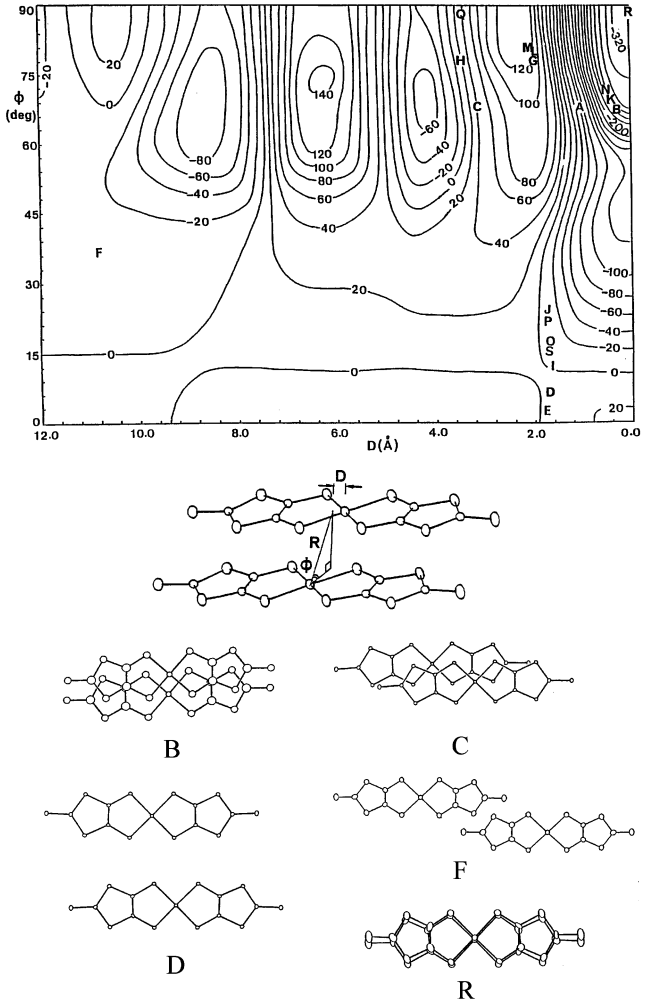

Figure 2. Map of LUMO···LUMO overlap integrals between two Ni(dmit)$_2$ molecules, as a function of intermolecular coordinates, D and ϕ. The symbols A, B, C, ... indicate observed arrangements. (Reprinted with permission from ref 118. Copyright 1987 Elsevier Sequoia.)

the first-principles band calculations for (Me_4N)-[M(dmit)$_2$]$_2$ (M = Ni, Pd) based on the density functional theory within the generalized gradient approximation yielded $\Delta = 0.73$ eV for Ni(dmit)$_2$ and $\Delta = 0.59$ eV for Pd(dmit)$_2$.[116] The Δ value for Pd(dmit)$_2$ was estimated to be 0.8−0.9 eV by optical studies.[117] The Δ value depends on the dithiolene ligand and the central metal. The Δ value of Pt(mnt)$_2$ calculated by the extended Hückel method is almost twice that of M(dmit)$_2$ (M = Ni, Pd).[6e] On the other hand, the calculated Δ values for M(dddt)$_2$ are almost equal to those for M(dmit)$_2$.

The intermolecular transfer integral which governs the electronic structure is approximately proportional to the intermolecular overlap integral. The magnitude and sign of the intermolecular overlap integral calculated from the crystal data strongly depend on the geometrical relation between the corresponding two molecules and the symmetry of the molecular orbital. Figure 2 shows the overlap integral ($\times 10^4$) of the LUMO between two Ni(dmit)$_2$ molecules as a function of the slipping (D) and the relative angle (ϕ).[118] In this calculation, the two molecules are arranged with their molecular planes parallel to each other. The R value in Figure 2 is assumed to be a minimum value for each (D, ϕ) under the restriction that no intermolecular atom pair is allowed to come within the sum of the van der Waals radii. Although the M(dmit)$_2$ has a molecular architecture similar to that of the organic donor BEDT-TTF, as mentioned in the previous section, the map for Ni(dmit)$_2$ is quite different from the corresponding map for the overlap integral of the HOMO between two BEDT-TTF molecules. In the BEDT-TTF compounds, the side-by-side configuration effectively enhances the transverse intermolecular interaction and provides 2D electronic structures.[119] In Figure 2, however, the corresponding side-by-side configurations of the Ni(dmit)$_2$ molecule ($D \sim 1.8$ Å) lead to very small overlap integrals for all ϕ values. This is because some of overlap integrals for the intermolecular S·· ·S pairs are canceled out due to the b_{2g} symmetry of the LUMO. On the other hand, since the HOMO of the M(dmit)$_2$ molecule has a symmetry similar to that of the HOMO of the BEDT-TTF molecule, the transverse HOMO···HOMO overlap integral can be enhanced in the side-by-side configuration.

Another aspect of the two-MO nature was discussed in the dimer system. Charge separation (charge ordering) is a widely observed phenomenon in conducting materials, including molecular conductors and transition metal oxides, and is a subject of intense research because of its crucial role in the electronic properties.[120] The conventional charge separation in the molecular system is driven by intersite electrostatic repulsions in the single-MO conductors. If molecules with the two-MO configuration are strongly dimerized, the HOMO−LUMO interplay can drive a new type of charge separation phenomenon due to local quantum resonance. This possibility was first proposed for the $[Pd(dmit)_2]_2^-$ dimer in the β' type anion radical salts, as a spontaneous charge separation (2 dimer$^-$ → dimer^0 + dimer^{2-}).[121] In this case, the energy cost of electron pairing within the dimer is largely reduced by forming a HOMO−LUMO double bond.

When we consider the electronic structure of the metal dithiolene compounds, the small HOMO−LUMO energy splitting and the difference in the symmetry between the HOMO and LUMO should always be kept in mind. Depending on molecular arrangements in crystals, these features provide a variety of electronic states.

3. Geometrical Aspect: Dimensionality, Dimerization, and Frustration

3.1. (Quasi-) One-Dimensional Systems

3.1.1. Parallel Band vs Crossing Band, Multisheet Fermi Surface

Acceptor type metal dithiolene complexes, M(mnt)$_2$, M(dmit)$_2$, and their Se-analogues, have planarity over the whole molecule and tend to stack in the face-to-face fashion. For example, in the first metallic metal dithiolene compound $(H_3O)_{0.33}Li_{0.8}[Pt(mnt)_2]\cdot 1.67H_2O$, the Pt(mnt)$_2$ molecules stack with an eclipsed configuration to form a uniform columnar

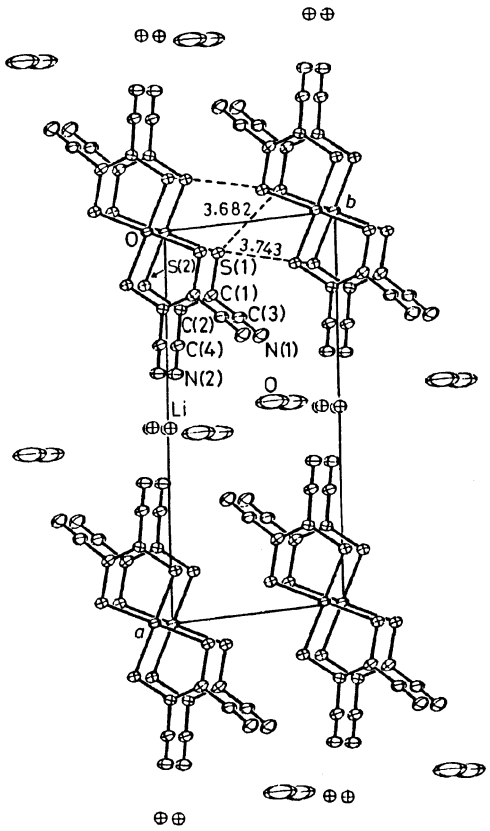

Figure 3. Crystal structure of $(H_3O)_{0.33}Li_{0.8}[Pt(mnt)_2]\cdot 1.67H_2O$. (Reprinted with permission from ref 39a. Copyright 1982 Royal Society of Chemistry.)

structure (Figure 3).[39a] There are short S···S distanced along the transverse direction. This compound undergoes a metal−insulator transition at about 220 K accompanied by the charge density wave (CDW) formation. The satellite spots associated with the CDW indicate that this compound has a partially (59%) filled 1D band. Since the HOMO−LUMO energy splitting Δ is not so small, the conduction band is a LUMO-based band. The intercolumn overlap integrals of the LUMO are much smaller than the intracolumn overlap integral, which leads to the 1D electronic structure.[39b]

An enhancement of the intercolumn interaction is a way to gain higher dimensional systems. Indeed, in the first organic superconducting system $(TMTSF)_2X$ where S atoms in the TTF skeleton are replaced with larger Se atoms, short Se···Se contacts enhance the intercolumn interaction up to about 1/10 of the intracolumn interaction. The Fermi surface of this system is a pair of distorted planes, and the density wave formation is suppressed. The intercolumn interaction, however, can give another type of effect on the electronic structure, as was discussed for $(DBTTF)[Ni(dmit)_2]$.[49] Let us consider a two-chain donor−acceptor (1:1 molar ratio) system with noninteracting segregated 1D columns. In each column, molecular units are repeated uniformly. According to the tight-binding picture, there are two energy bands near the Fermi level; a HOMO-based band associated with the donor column and a LUMO-based band associated with the acceptor column. There are two types of band structure, depending on the sign of the intracolumn transfer integral (Figure 4). The

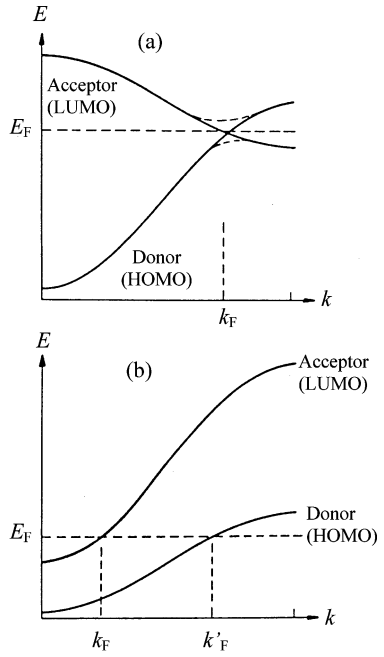

Figure 4. Crossing band (a) and parallel band (b).

one is the "crossing" band structure composed of normal and inverted 1D bands, and the other is the "parallel" band structure where both 1D bands are normal (or inverted). In the crossing band structure, the signs of intracolumn HOMO···HOMO and LUMO···LUMO transfer integrals are different. An example is TTF-TCNQ. When the signs of the intracolumn transfer integrals are the same, the system has the parallel band structure, as is the case of (DBTTF)-$[Ni(dmit)_2]$. The sign of the intracolumn transfer integral depends on the overlapping mode and the symmetry of the frontier orbital. In the crossing band system, the two bands cross at the Fermi wavenumber k_F. Therefore, if the intercolumn interaction between unlike columns is introduced, a covalency gap develops at the Fermi level, yielding a (narrow-gap) semiconductor. Indeed, the first-principles band calculation for TTF-TCNQ indicated the energy gap formation and resultant hole- and electron-like Fermi surfaces due to the small but significant intercolumn interaction between the TTF and TCNQ columns.[122] This feature has been confirmed by angle-resolved photoemission spectroscopy.[123] On the other hand, in the parallel band system, the intercolumn interaction between unlike columns does not form the energy gap. Of course, in the simple parallel band system as shown in Figure 4, there still remains the instability of the metallic state associated with the planar Fermi surface if the intercolumn interactions between like and unlike columns are not effectively strong.

Such a situation is not limited only to the donor−acceptor system. In the molecular design for the (stoichiometrically) single-component molecular metals based on the metal dithiolene complexes, a similar issue was discussed.[124] Even in the single-component molecular crystal, internal electron transfer between the HOMO and LUMO bands can occur, if the HOMO−LUMO energy splitting is small enough. This generates partially filled energy bands and leads

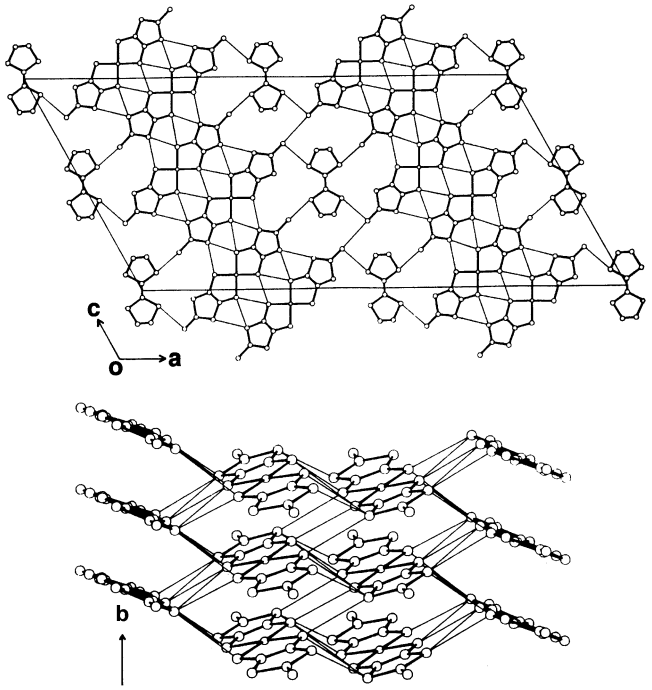

Figure 5. Crystal structure of (TTF)[Ni(dmit)$_2$]$_2$. (Reprinted with permission from ref 48a. Copyright 1986 American Chemical Society.)

to a (semi)metallic state.[6e] In this sense, the single-component molecular metal is a multiband system. One can notice that possible band structures are also illustrated schematically in Figure 4. Therefore, in the crossing band case, the HOMO···LUMO interaction removes the Fermi surface. If the higher dimensional HOMO···HOMO and/or LUMO···LUMO interactions are introduced, the Fermi surface survives even in the presence of the HOMO···LUMO interaction. Indeed, the first single-component molecular metal Ni(tmdt)$_2$ (tmdt = trimethylenetetrathiafulvalenedithiolate) reported in 2001 has the crossing type band structure and exhibits 3D hole- and electron-like Fermi surfaces.[125] Another approach is the formation of the parallel band structure which is stable against the HOMO−LUMO interaction and generates large Fermi surfaces derived from both the HOMO and LUMO bands. For this purpose, an important factor is the tuning of the overlap mode.[124]

We now return to the donor−acceptor type compounds. The first superconductor based on the metal dithiolene complex (TTF)[Ni(dmit)$_2$]$_2$ is thought to be a 1D system with the parallel band structure. Figure 5 shows the crystal structure with the space group *C*2/*c*. The crystal consists of uniform TTF and Ni(dmit)$_2$ columns. Intercolumn HOMO···HOMO and (TTF) LUMO···LUMO (Ni(dmit)$_2$) interactions are much smaller than intracolumn ones, which indicates a strong 1D nature of the electronic structure.[118] The unit cell reduced to the primitive one contains two TTF molecules and four Ni(dmit)$_2$ molecules. Therefore, in the vicinity of the Fermi level, there are one HOMO (TTF) band and two LUMO (Ni(dmit)$_2$) bands, each of which is almost doubly degenerate. In addition, it has been pointed out that there exist partially filled HOMO (Ni(dmit)$_2$) bands near the HOMO (TTF) band, which is due to the small HOMO−LUMO energy splitting in the Ni(dmit)$_2$ molecule and

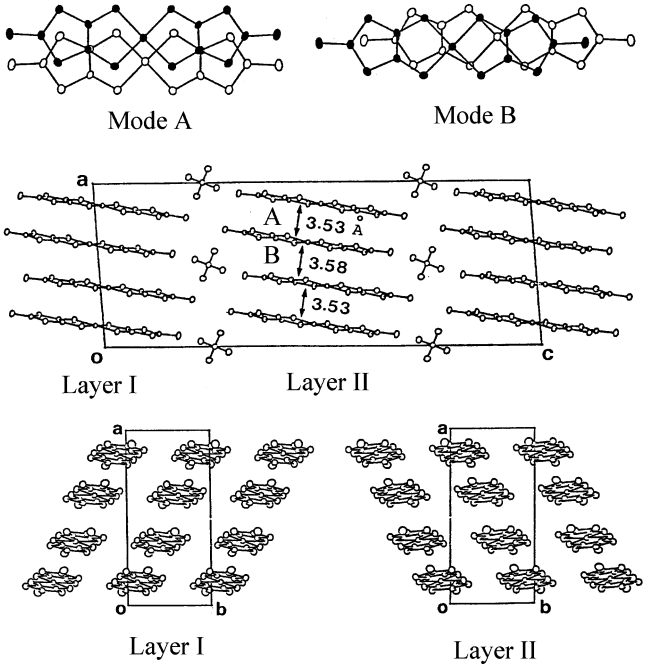

Figure 6. Crystal structure of (Me$_4$N)[Ni(dmit)$_2$]$_2$.

is consistent with the result of the X-ray diffuse scattering experiments.[22] The electronic structure of this system is characterized by the multisheet Fermi surface. In general, if one part of the Fermi surface fits into another part by the translation vector **q** in the reciprocal space, it is said that the Fermi surface "nests" and **q** is the nesting vector. The instability of the conventional 1D metallic system accompanied by the density wave formation is associated with the shape of its Fermi surface (a set of parallel sheets) which nests completely with a single **q** (=2k_F). In the multisheet Fermi surface system, however, complete nesting of the Fermi surface with a single **q** is impossible. The X-ray diffuse scattering experiments for (TTF)[Ni(dmit)$_2$]$_2$ show complicated CDW formation associated with the nesting of the multisheet Fermi surface at low temperatures.[48b] The temperature dependence of the resistivity, however, remains metallic and exhibits no anomaly down to 1.5 K. This is the most unusual feature of this system and remains an open question. The electronic structure of α′-(TTF)[Pd(dmit)$_2$]$_2$ is similar to that of (TTF)[Ni(dmit)$_2$]$_2$. In contrast to (TTF)[Ni(dmit)$_2$]$_2$, this system is nonmetallic below about 220 K at ambient pressure, which is consistent with the development of CDW instabilities at low temperatures.[48b] This sharp difference between (TTF)[Ni(dmit)$_2$]$_2$ and α′-(TTF)[Pd(dmit)$_2$]$_2$ in the conducting behavior, despite being isostructural, has not been fully understood.

3.1.2. Solid Crossing Column Structure

The solid crossing column structure is one of the typical molecular arrangements in the M(dmit)$_2$ salts. (Me$_4$N)[Ni(dmit)$_2$]$_2$ is the first π acceptor-based conductor with the closed-shell cation which exhibits superconductivity.[13,59] In the crystal with the space group *C*2/*c*, the unit cell contains two crystallographically equivalent Ni(dmit)$_2$ layers (I and II, Figure 6) parallel to the *ab* plane. These anion layers are separated from each other by the cation sheet.

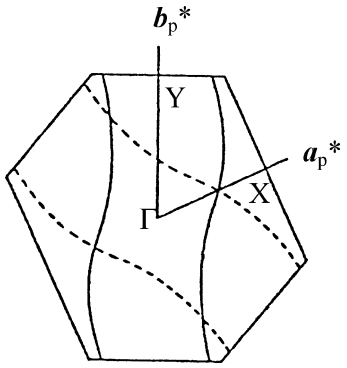

Figure 7. Calculated Fermi surface of $(Me_4N)[Ni(dmit)_2]_2$.

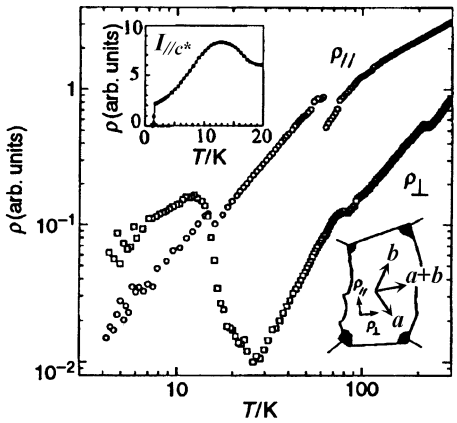

Figure 8. Anisotropy of the resistivity of α-(EDT-TTF)-[Ni(dmit)$_2$]. The inset shows the superconducting transition at 1.3 K. (Reprinted with permission from ref 50b. Copyright 1995 Royal Society of Chemistry.)

In each anion layer, the Ni(dmit)$_2$ units stack to form a columnar arrangement with independent interplanar distances of 3.53 and 3.58 Å. The Ni(dmit)$_2$ columns in the same layer are parallel but lie crisscross with those in the adjacent layer, owing to the glide plane along the *c* axis; the stacking direction is along the $a + b$ direction in layer I and along the $a - b$ direction in layer II. In this compound, the band structure near the Fermi level is described by the LUMO band and has a 1D nature. Values of intracolumn overlap integrals of the LUMO indicate that Ni(dmit)$_2$ units are weakly dimerized in the column. The Fermi surface obtained by the tight-binding band calculation is shown in Figure 7. This Fermi surface consists of two pairs of distorted sheets which are equivalent but open to different directions owing to the solid crossing column structure. Therefore, (Me_4N)-[Ni(dmit)$_2$]$_2$ is a kind of the multisheet Fermi surface system. At ambient pressure, this compound shows the metallic temperature dependence of the resistivity down to about 100 K, where a resistivity jump occurs. Below 20 K, a sharp upturn of the resistivity is observed. The polarized reflectance spectra show Drude-like behavior down to 20 K.[126] The anisotropy of the plasma frequency within the *ab* plane suggests that this compound has a strong 1D character along the stacking direction. An application of hydrostatic pressure reduces two types of resistivity anomalies at 100 and 20 K, and the sample where the 20 K anomaly is suppressed exhibits superconductivity at 3.0 K under 3.2 kbar. The transition temperature rises with increasing pressure up to 5.0 K (under 7 kbar). $(Me_3Te)[Ni(dmit)_2]_2$ also exhibits the solid crossing column structure.[70] Its electronic structure is largely modified by the intermolecular Te···S contacts between the cation and the terminal thione group in the Ni(dmit)$_2$ anion, as mentioned in section 5.

Some M(dmit)$_2$ salts with organic donors exhibit slightly different types of solid crossing column structures. α-(EDT-TTF)[Ni(dmit)$_2$] (EDT-TTF = ethylenedithiotetrathiafulvalene) is the only ambient-pressure superconductor derived from the metal dithiolene complex.[14,50] The crystal belongs to the triclinic system with the space group $P\bar{1}$. EDT-TTF molecules stack in the head-to-tail manner along the $a + b$ direction and are weakly dimerized. Ni(dmit)$_2$ molecules on the inversion centers form a uniform column along the *b* direction. The calculated Fermi surface assuming the degree of charge transfer $^1/_2$ consists of two pairs of warped planes which are associated with the HOMO band (the EDT-TTF layer) and the LUMO band (the Ni(dmit)$_2$ layer), respectively. Due to the difference of the two types of columns in the stacking direction, these pairs are orientated differently and are not completely nested by a single modulation wave vector. It should be noted that a 2D band associated with the HOMO of the Ni(dmit)$_2$ molecule is possibly located near the Fermi level. Even in this case, there are two pairs of warped planes with different orientations when the charge-transfer value is around $^1/_2$ and the HOMO−LUMO energy splitting Δ is assumed to be 0.68 eV.[50b] At ambient pressure, the electrical resistivity along the $a + b$ direction decreases monotonically down to 20 K. Below 20 K, the resistivity increases on cooling and shows a peak around 14 K (Figure 8). Along the direction almost perpendicular to this direction, on the other hand, the resistivity anomaly is small. The resistance along the c^* direction is weakly temperature dependent, showing a broad maximum around 120 K. The resistance anomaly is also observed as a peak around 12 K. This system undergoes a superconducting transition at 1.3 K. The angle dependence of the weak-field magnetoresistance within the conduction plane indicates that the electrical conduction is associated mainly with the Ni(dmit)$_2$ column below 10 K, whereas both the EDT-TTF and Ni(dmit)$_2$ columns contribute to the electrical conduction above 20 K.[127] This suggests that the low-temperature anomaly is due to the density wave (probably spin density wave) formation on the EDT-TTF column and the superconductivity below 1.3 K coexists with the density wave. In contrast to α-(EDT-TTF)[Ni(dmit)$_2$], γ-(EDT-TTF)[Ni(dmit)$_2$] has a parallel column structure where both the EDT-TTF and Ni(dmit)$_2$ columns are parallel to the *c*-axis direction.[50b] At ambient pressure, the resistivity of this compound shows a metallic temperature dependence down to 100 K, where a gradual transition into an insulator occurs.

The solid crossing column structure is also observed in other anion radical salts of M(dmit)$_2$ (M = Pd, Pt) and its Se-analogues, including α,β-(Me_4N)-[Pd(dmit)$_2$]$_2$,[83] β′-(Me_4Z)[Pd(dmit)$_2$]$_2$ (Z = P, As, Sb),[85] β′-(Et_2Me_2Z)[Pd(dmit)$_2$]$_2$ (Z = P, As, Sb),[86] Cs[Pd-(dmit)$_2$]$_2$,[94] (Me_3Te)[Pd(dmit)$_2$]$_2$,[91] (quinuclidinium)-

$[Pd(dmit)_2]_2$,[93] β'-$(Me_4Z)[Pd(dmise)_2]_2$ (Z = P, As, Sb),[85] β-$(Me_4N)[Pd(dsit)_2]_2$,[105] and $(Me_4N)[Pt(dmit)_2]_2$.[96] The electronic structures of these Pd and Pt salts, however, are very different from that of $(Me_4N)[Ni(dmit)_2]_2$, owing to the strong dimerization (vide infra).

3.2. Higher Dimensional Systems

3.2.1. Spanning Overlap

In the development of molecular conductors with higher dimensional (2D or 3D) electronic structures, the organic donor BEDT-TTF played a crucial role.[1,4] This molecule removed a prejudice that the π-conjugated molecules prefer the face-to-face stacking structure. Indeed, a variety of 2D systems have been derived from noncolumnar arrangements of BEDT-TTF molecules. Important features of the BEDT-TTF molecule are (1) the outer six-membered heterorings that expand the TTF skeleton and enhance intermolecular S···S contacts in the transverse direction, and (2) the terminal ethylene groups that exhibit flexible conformations and prevent infinite face-to-face stacking.

On the other hand, acceptor type metal dithiolene complexes tend to stack in the face-to-face fashion. As mentioned in section 2, the symmetry of the LUMO reduces the transverse intermolecular interactions, which is not favorable for the formation of higher dimensional electronic structures. The spanning overlap of the $M(dmit)_2$ molecules, however, has shown another route to the higher dimensional system based on the face-to-face stacking architecture.[11] α-$Et_2Me_2N[Ni(dmit)_2]_2$ is the first 2D metal derived from the π-acceptor molecule. Figure 9 shows the crystal structure. The repeating unit along the *c* axis consists of four $Ni(dmit)_2$ molecules (A, B, C, and D). There are two types of overlapping modes, I (A···B, C···D) and II (B···C, A···D′). Mode I, the spanning overlap where *one* molecule overlaps with *two* molecules, forms a 2D conduction path parallel to the *bc* plane. The Fermi surface of this compound was found to be two-dimensional.[60] The spanning overlap mode is also observed in γ-$(Et_2Me_2N)[Ni(dmit)_2]_2$,[62] (acridinium)$[Ni(dmit)_2]_3$,[71] (*N*,*N*-dimethylpiperidinium)-$[Ni(dmit)_2]_2$,[65] and (*N*,*N*-dimethylpiperidinium)$[Ni(dmise)_2]_2$.[104] All these compounds exhibit metallic resistivity behavior down to low temperatures. Despite the normal metallic behavior observed in the resistivity measurements, an unexpectedly large and temperature-dependent magnetic susceptibility has been reported for α-$(Et_2Me_2N)[Ni(dmit)_2]_2$, (*N*,*N*-dimethylpiperidinium)$[Ni(dmit)_2]_2$, and (*N*,*N*-dimethylpiperidinium)$[Ni(dmise)_2]_2$.[104] This suggests that the metallic state associated with the spanning overlap molecular arrangement cannot be explained by the simple metal model.

Large and planar molecules where the π-conjugated system extends spaciously over the molecular plane are suitable for the spanning overlap. The first single-component molecular metal $Ni(tmdt)_2$ demonstrates the 3D electronic structure associated with the spanning overlap and the transverse intermolecular interaction.[124,125] The $Ni(tmdt)_2$ molecule includes extended π ligands having a TTF skeleton. In the crystal, the long and planar $Ni(tmdt)_2$ molecule spans the adjacent molecules with the face-to-face overlap. The intermolecular overlap integrals among frontier orbitals (HOMO···HOMO, LUMO···LUMO, and HOMO···LUMO) exhibit small anisotropy. Therefore, this system has a 3D Fermi surface.

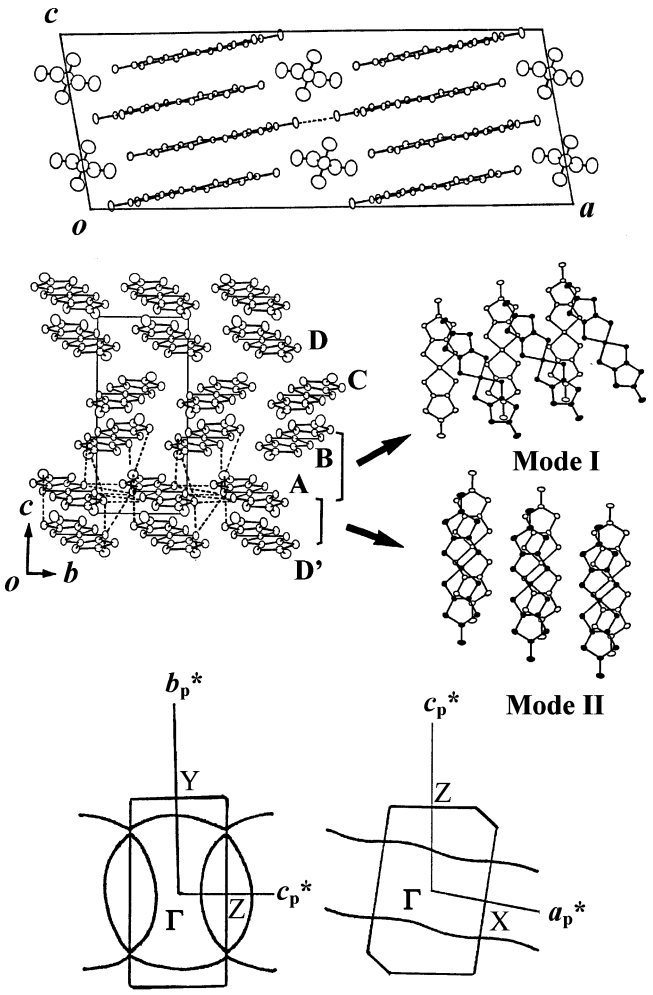

Figure 9. Crystal structure and calculated Fermi surface of α-$(Et_2Me_2N)[Ni(dmit)_2]_2$. The *C*-centered monoclinic cell is reduced to the primitive one as $a_p = (a + b)/2$, $b_p = -b$, $c_p = -c$.

Molecular design toward the spanning overlap type of molecular arrangement has been examined for phthalocyanine neutral radicals and partially oxidized salts.[128] An introduction of axial ligands (CN^-) to the planar phthalocyanines prevents the simple 1D stacking and leads to a variety of $\pi-\pi$ stacking networks based on the spanning overlap. The dimensionality of the electronic system can be tuned by the choice of the second component, the crystal solvent in the neutral radical crystal or the cation in the partially oxidized salt crystal. In many cases, interactions between the second component and the axial ligands determine the crystal structure.

3.2.2. Dimerization: HOMO–LUMO Band Inversion

In the conducting anion radical salts of $M(dmit)_2$, dimerization plays a crucial role in determining the electronic structure and therefore the electronic properties. A typical example is β-$(Me_4N)[Pd(dmit)_2]_2$

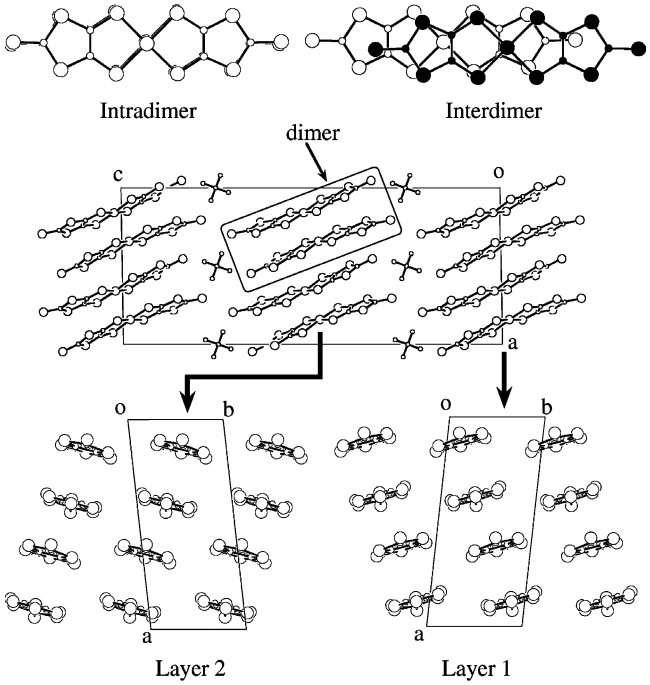

Figure 10. Crystal structure of β-$(Me_4N)[Pd(dmit)_2]_2$.

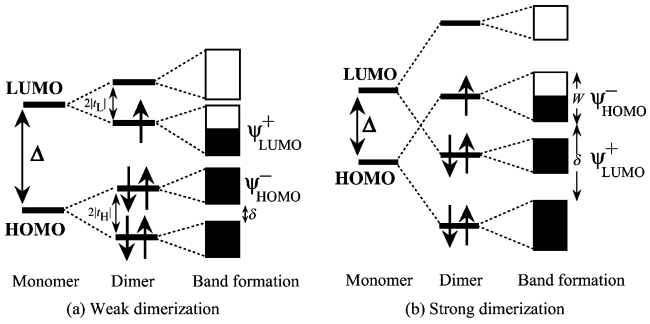

Figure 11. Schematic electronic structures for dimerized metal dithiolene systems.

and related $Pd(dmit)_2$ salts.[17,83,84] The crystal structure of β-$(Me_4N)[Pd(dmit)_2]_2$ is similar to that of $(Me_4N)[Ni(dmit)_2]_2$ (Figure 10). In the crystal with the space group $C2/c$, the $Pd(dmit)_2$ molecules form the solid crossing columns interrelated by the glide plane. Two crystallographically equivalent conduction layers (1 and 2) are separated by the insulating cation layer. In contrast to the Ni salt, the $Pd(dmit)_2$ molecules are strongly dimerized in each column. Within the dimer, two $Pd(dmit)_2$ molecules overlap in an eclipsed mode and a short intermolecular Pd···Pd distance (3.116 Å) is observed. The intra- and interdimer separations within the column are 3.28 and 3.81 Å, while they are close to each other in the Ni salt (3.53 and 3.58 Å).

Let us consider an effect of the dimerization on the electronic structure. Within the isolated dimer, each HOMO and LUMO in the monomer generates bonding and antibonding combinations separated by $2|t_H|$ and $2|t_L|$, where t_H and t_L are intermonomer HOMO···HOMO and LUMO···LUMO transfer integrals within the dimer, respectively (Figure 11). Since the HOMO−LUMO energy splitting Δ is small, there are two different possibilities for the energy level ordering of the dimer depending on the degree of the dimerization. If $|t_H|$ and $|t_L|$ are smaller than $\Delta/2$ (weak dimerization condition), the antibonding combination of the HOMOs is lower than the bonding combination of the LUMOs. On the other hand, if $|t_H|$ and $|t_L|$ are larger than $\Delta/2$ (strong dimerization condition), the antibonding combination of the HOMOs is *higher* than the bonding combination of the LUMOs and a "HOMO−LUMO level inversion" occurs. It is considered that β-$(Me_4N)[Pd(dmit)_2]_2$ is in the strong dimerization condition while $(Me_4N)[Ni(dmit)_2]_2$ is in the weak dimerization condition.

Next, with the above picture in mind, we consider a 1D column (along the a direction) of the dimerized $[M(dmit)_2]^{1/2-}$ units as a basic model for the present system. The simple tight-binding band model indicates that each HOMO and LUMO with an energy of E_0 forms two energy bands $E(k) = E_0 \pm [t_A^2 + t_B^2 + 2t_A t_B \cos ka]^{1/2}$, where t_A is the intradimer transfer integral ($= t_H$ or t_L) and t_B is the interdimer transfer integral ($|t_A| > |t_B|$). This means that the dimerization generates the upper (ψ^-; antibonding) and lower (ψ^+; bonding) bands separated by an energy gap $\delta = 2(|t_A| - |t_B|)$ and the energy level E_0 is located in the middle of the energy gap. The bandwidth of each band is $2|t_B|$. When the dimerization is strong ($|t_A| \gg |t_B|$), the upper and lower bands are largely separated by the dimerization gap δ and both bands are effectively very narrow. When the HOMO−LUMO level inversion occurs within the dimer, the antibonding HOMO band ψ^-_{HOMO} will be located higher than the bonding LUMO band ψ^+_{LUMO} (Figure 11). In this HOMO−LUMO band inversion case, the formal charge of $-1/2$ indicates that the ψ^-_{HOMO} band forms the conduction band and is effectively half-filled (Figure 11). These features are not largely affected by an introduction of intercolumn interactions. As mentioned in section 2, the transverse HOMO···HOMO interaction of the $M(dmit)_2$ molecule is stronger than the transverse LUMO···LUMO interaction. Therefore, the tight-binding calculation indicated that β-$(Me_4N)[Pd(dmit)_2]_2$ has a 2D electronic structure where the Fermi surface consists of two cylinders associated with conduction layers 1 and 2. It should be added that the bandwidth of the ψ^-_{HOMO} band is wider than that of the ψ^+_{LUMO} band, due to stronger transverse interactions. The results of the first-principles band calculations for $(Me_4N)[M(dmit)_2]_2$ (M = Ni, Pd) based on the density functional theory within the generalized gradient approximation agree with the above-mentioned picture (Figure 12).[116] The existence of the HOMO−LUMO band inversion has been experimentally confirmed by the polarized reflectance spectra for analogous salts, β'-$(Me_4As)[Pd(dmit)_2]_2$ and $Cs[Pd(dmit)_2]_2$.[117] β-$(Me_4N)[Pd(dmit)_2]_2$ shows no clear metallic behavior at ambient pressure, which indicates that this system is a Mott insulator. The application of pressure higher than 5 kbar induces a metallic behavior, and a superconducting transition occurs at 6.2 K under 6.5 kbar.[17,84] It should be added that α-$(Me_4N)[Pd(dmit)_2]_2$ has a crystal structure similar to that of the β-form but the application of pressure cannot suppress the nonmetallic behavior up to 12 kbar. An important structural difference is that the α-Me_4N salt belongs to the triclinic system and the two conduction layers are crystallographi-

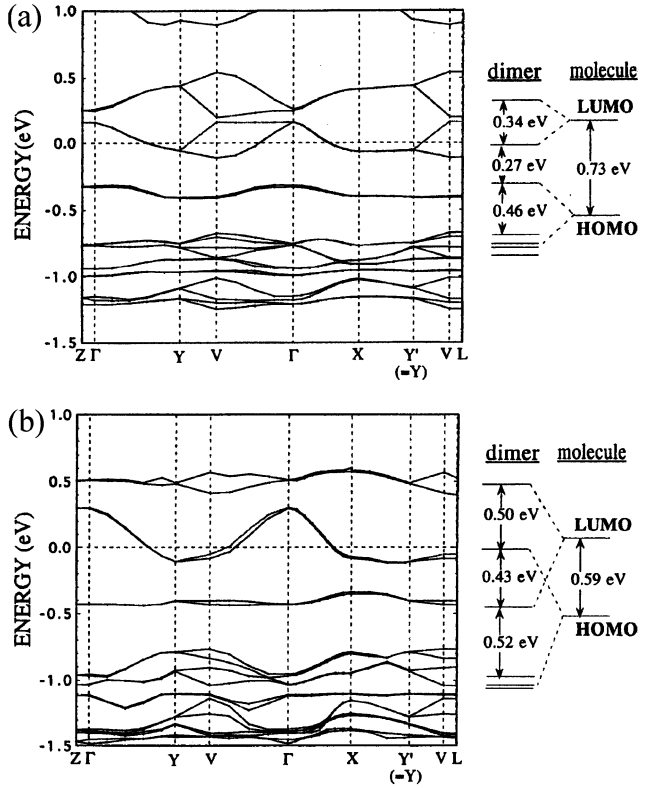

Figure 12. Band structures of $(Me_4N)[Ni(dmit)_2]_2$ (a) and β-$(Me_4N)[Pd(dmit)_2]_2$ (b) obtained by first-principles band calculations. (Reprinted with permission from ref 116. Copyright 1999 American Physical Society.)

cally nonequivalent. A possible effect of such a symmetry breaking on the electronic state will be discussed in section 4.2.

In the systems with the small HOMO−LUMO energy splitting Δ, the conduction band can originate either from the LUMO for weakly dimerized systems or from the HOMO for strongly dimerized systems. Depending on the original MO character, the dimensionality of the electronic structure can be either 2D for the HOMO-based band (ψ^-_{HOMO}) or 1D for the LUMO-based band (ψ^+_{LUMO}). β-$(Me_4N)[Pd(dmit)_2]_2$ and related $Pd(dmit)_2$ salts are the former case and $(Me_4N)[Ni(dmit)_2]_2$ is the latter case. The strong dimerizations of the $Pd(dmit)_2$ salts are associated with the eclipsed stacking mode of the monomers, which is very favorable for the pσ−pσ type S···S overlap. For the eclipsed stacking mode, the central metal plays a crucial role.[6e,6g,116,129] The metal d_{xz} orbital contributes to the LUMO of the monomer, and the bonding combination of the LUMOs has some metal−metal bonding character. The larger spatial extension of the d orbitals of the Pd atom stabilizes this metal−metal bonding and relieves the excessive S···S repulsions. The weaker bonds between the Pd atom and the dmit ligands are responsible for the smaller energy cost in the bending away of the ligands at the metal site so as to relieve the steric hindrance. The smaller Δ value due to the weaker metal−ligand bonds supports the HOMO−LUMO level inversion and leads to the double occupancy of the bonding combination of the LUMOs, which stabilizes the eclipsed stacking mode.

The $Pd(dmit)_2$ salt with the organic donor α'-(EDT-TTF)[$Pd(dmit)_2$] exhibits a solid crossing column structure with the EDT-TTF column along the a-axis direction and the $Pd(dmit)_2$ column along the $a + c$ direction.[81] The $Pd(dmit)_2$ anions are strongly dimerized in the column. Consequently, the conduction band is built from the HOMO of $Pd(dmit)_2$ and the HOMO of EDT-TTF. Similar to α-(EDT-TTF)[Ni-$(dmit)_2$], this compound shows a metallic behavior accompanied by a resistivity peak around 40 K. The application of pressure suppresses the resistivity anomaly at 5 kbar. No indication of the superconductivity, however, was found down to 400 mK and up to 10 kbar. The magnetic susceptibility and X-ray diffuse scattering measurements revealed that the resistivity anomaly is associated with the CDW formation on the EDT-TTF column. Comparison between the observed CDW wave vector and the nesting vector for the calculated Fermi surface suggests that the charge-transfer value is about $^3/_4$. For this charge-transfer value, the Fermi surface consists of a pair of warped planes associated with the EDT-TTF layer and a cylinder associated with the Pd-$(dmit)_2$ layer. On the other hand, γ-(EDT-TTF)[Pd-$(dmit)_2$] has the parallel column structure where EDT-TTF and $Pd(dmit)_2$ molecules form segregated columns parallel to the a axis.[50b] In the triclinic crystal, EDT-TTF and $Pd(dmit)_2$ conduction layers parallel to the ac plane are arranged alternately. The $Pd(dmit)_2$ molecules are strongly dimerized within the column. At ambient pressure, the resistivity perpendicular to the $a + c$ direction is metallic down to 100 K and shows an upturn at 80 K followed by a broad maximum around 50 K, while the resistivity parallel to the $a + c$ direction shows a metal−semimetal transition at about 50 K. X-ray diffuse scattering measurements and tight-binding band calculations indicate that the resistivity anomaly is associated with the CDW formation due to the partial nesting of the anisotropic 2D Fermi surface.

In contrast to the $M(dmit)_2$ (M = Ni, Pd, Pt, Au) molecules, the $M(dddt)_2$ molecules belong to the electron donor group. The $M(dddt)_2$ molecule is a metal complex analogue of the organic donor BEDT-TTF. Formally, the central C=C bond of BEDT-TTF is substituted by a metal ion in the $M(dddt)_2$ molecule. The HOMO and LUMO of $M(dddt)_2$ are very similar in orbital character to those of $M(dmit)_2$. In addition, the HOMO of $M(dddt)_2$ is also very similar to that of BEDT-TTF. Since the HOMO−LUMO energy splitting of $M(dddt)_2$ is small, the strong dimerization can cause the HOMO−LUMO band inversion in the $M(dddt)_2$ compounds. For the donor system, however, the situation is quite different. The formal charge of $+^1/_2$ (one hole per dimer) is the frequently observed valence state in the donor system and corresponds to the $-^1/_2$ valence state (one electron per dimer) in the acceptor system. For the donor system with this valence state, the HOMO−LUMO band inversion results in a half-filled LUMO-based band ψ^+_{LUMO} as the conduction band. This is the case of $[Pt(dddt)_2]AuBr_2$.[130] The crystal structure of this compound is similar to that of β-$(BEDT\text{-}TTF)_2IBr_2$. The triclinic unit cell contains two $Pt(dddt)_2$ cations

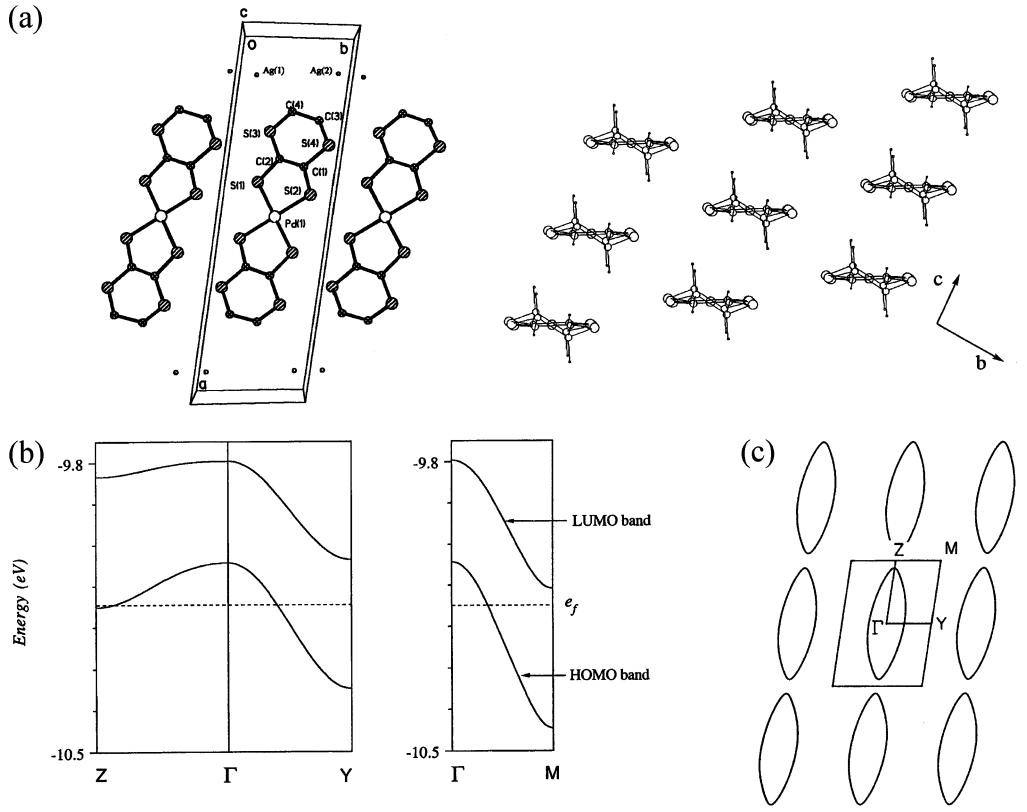

Figure 13. Crystal structure (a), band structure (b), and calculated Fermi surface for an assumed formal charge of $+^1/_2$ (c) of $[Pd(dddt)_2]Ag_{1.54}Br_{3.50}$. (Reprinted with permission from ref 110. Copyright 1996 EDP Sciences.)

which are strongly dimerized in the eclipsed fashion with a short Pt···Pt distance (2.98 Å). The ψ^+_{LUMO} band is very narrow, which is an origin of semiconducting behavior. $[Pt(dddt)_2]IBr_2$ is isostructural with $[Pt(dddt)_2]AuBr_2$.[107b] This salt demonstrates an example of the intermediate dimerization with an intradimer Pt···Pt distance of 3.36 Å. The tight-binding band calculation indicates that the ψ^+_{LUMO} band largely overlaps with the ψ^-_{HOMO} band.[130] This salt is a semiconductor, but the electrical conductivity is higher than that of $[Pt(dddt)_2]AuBr_2$. A remarkable example of the system with no dimerization is $[Pd(dddt)_2]Ag_{1.54}Br_{3.50}$.[110] The triclinic unit cell contains only one $Pd(dddt)_2$ cation (Figure 13a). The Ag and Br atoms are disordered, occupying four and six positions, and form nonstoichiometric silver bromide anions. The $Pd(dddt)_2$ cations stack uniformly along the *c* axis with the interplanar distance 3.84 Å. In the stack, the adjacent cations are displaced along the short axis of the molecule. Calculated intermolecular transfer integrals indicate that the strongest interaction is observed along the *b*-axis direction rather than along the *c*-axis direction. The HOMO-based band slightly overlaps with the LUMO-based band, but the Fermi level does not cut the LUMO-based band (Figure 13b). This means that the conduction band originates mainly from the HOMO. The calculated Fermi surface assuming the formal charge of $+^1/_2$—which means that almost all the silver atoms are in the Ag^{2+} oxidation state—has a 2D nature characterized by an ellipsoid shape (Figure 13c). For the formal charge of $Pd(dddt)_2$ between +0.25 and +0.55, the calculated Fermi surface retains the ellipsoid shape. This salt is a stable metal down to 1.3 K.

3.2.3. Quasi-Triangular Lattice: Spin Frustration

An isostructural series of β' type anion radical salts of $Pd(dmit)_2$ with tetrahedral cations, β'-$(Me_4Z)[Pd(dmit)_2]_2$ and β'-$(Et_2Me_2Z)[Pd(dmit)_2]_2$ (Z = P, As, Sb), is similar to β-$(Me_4N)[Pd(dmit)_2]_2$.[85b] Two crystallographically equivalent conduction layers (1 and 2) in the *C*-centered unit cell are interrelated to each other by the glide plane, and the $[Pd(dmit)_2]_2$ dimers stack along the $a + b$ direction in layer 1 and along the $a - b$ direction in layer 2, respectively. Compared with the β-Me_4N salt, these salts show some obvious differences in the positional interrelations between the dimer and the cation. However, the fundamental molecular arrangement within the conduction layer is the same. Calculated Fermi surfaces indicate that this system is a 2D system associated with the HOMO-based band (ψ^-_{HOMO}). This conduction band is narrow and half-filled. At ambient pressure, all these salts are nonmetallic due to the strong on-site Coulomb repulsion. In this Mott insulating state, one electron is located on each dimer $[Pd(dmit)_2]_2^-$.

As mentioned in section 3.2.2, the band structure near the Fermi level can be described by the HOMO-based band (ψ^-_{HOMO}). Furthermore, in the molecular conductors with strongly dimerized structure, one can generally extract the essence by taking each dimer as an effective unit.[27] The present β' type $Pd(dmit)_2$ system is also the case.[131] Table 8 shows an intradimer HOMO···HOMO transfer integral (t_A) and interdimer transfer integrals for the antibonding combination of the HOMOs (t_B, t_s, and t_r). These

Table 8. Intradimer HOMO···HOMO Transfer Integral (t_A), Interdimer Transfer Integrals for the Antibonding Combination of the HOMOs (t_B, t_s, and t_r), and Néel Temperature (T_N) for β'-(cation)[Pd(dmit)$_2$]$_2$

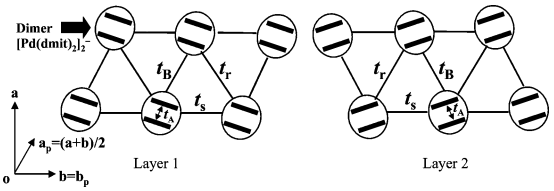

cation	type	T_N/K	t_A/meV	t_B/meV	t_s/meV	t_r/meV
Me_4P	A	42	439.5	36.4	33.7	21.5
Me_4As	A	35	443.5	34.0	32.6	22.8
Et_2Me_2P	B	17	445.8	29.4	29.3	24.3
Me_4Sb	B	16	450.1	30.0	28.4	25.4
Et_2Me_2As	C	16	446.6	29.6	29.3	24.4
Et_2Me_2Sb	C	<4.2	445.7	25.9	25.5	26.1

intra- and interdimer interactions exhibit the relation $t_A \gg t_B \approx t_s > t_r$ and can be tuned by the choice of the cation. The ratio t_r/t_B ranges from 0.6 to almost 1, while the ratio t_s/t_B remains around 1. An important point is that the dimers form a quasi-triangular lattice within the conduction layer. In the dimer model, the two branches of the conduction band associated with layers 1 and 2 are described as follows:

$$E_1(k) = 2.0[t_B \cos ka_p + t_r \cos k(a_p - b_p) + t_s \cos kb_p]$$

$$E_2(k) = 2.0[t_B \cos k(a_p - b_p) + t_r \cos ka_p + t_s \cos kb_p]$$

where the C-centered monoclinic cell is reduced to the primitive one as $a_p = (a + b)/2$, $b_p = b$, and $c_p = c$. This simple dimer model well reproduces the energy band structure around the Fermi level derived from the calculation including the HOMO and LUMO (Figure 14). The interdimer transfer integrals t_B, t_s, and t_r determine the dispersion of the energy band, while the effective on-site Coulomb energy on the dimer ($U_{eff.}$) is approximately correlated with the intradimer transfer integral t_A.[132] The bandwidth (W) is determined mainly by the two large interdimer transfer integrals t_B and t_s, and the smallest transfer integral t_r determines the anisotropy of the electronic structure.

The magnetic properties in the Mott insulating state are of special interest.[26] Each temperature dependence of the static magnetic susceptibility χ for this system usually exhibits a broad peak around ~100 K. The essential feature of the $\chi-T$ curve in the high-temperature region can be well explained by the high-temperature expansion calculations using the Padé approximants for the 2D spin-$^1/_2$ Heisenberg antiferromagnet on the triangular lattice (Figure 15). Other models including the spin-$^1/_2$ Heisenberg antiferromagnet on the 2D square lattice, and the spin-$^1/_2$ Heisenberg chain antiferromagnet cannot explain the observed behavior at all. This indicates that spin frustration operates in these salts.

Most of these salts undergo antiferromagnetic ordering at lower temperatures. An interesting point is that the Néel temperature T_N is correlated with the ratio t_r/t_B.[133] The system with the lower t_r/t_B ratio tends to exhibit the higher T_N, while the Et_2Me_2Sb salt with $t_r/t_B \sim 1$ shows no magnetic ordering down to 4.3 K.[134] In general, the exchange coupling J is proportional to $t^2/U_{eff.}$, where t is the interdimer transfer integral. Consequently, the ratio t_r/t_B is related to the deviation of the exchange coupling from the regular triangular model. Depending on the anisotropy of the interdimer interaction, the regular triangular lattice can be transformed into two important limits, the 2D square lattice ($t_r/t_B \rightarrow 0$ with

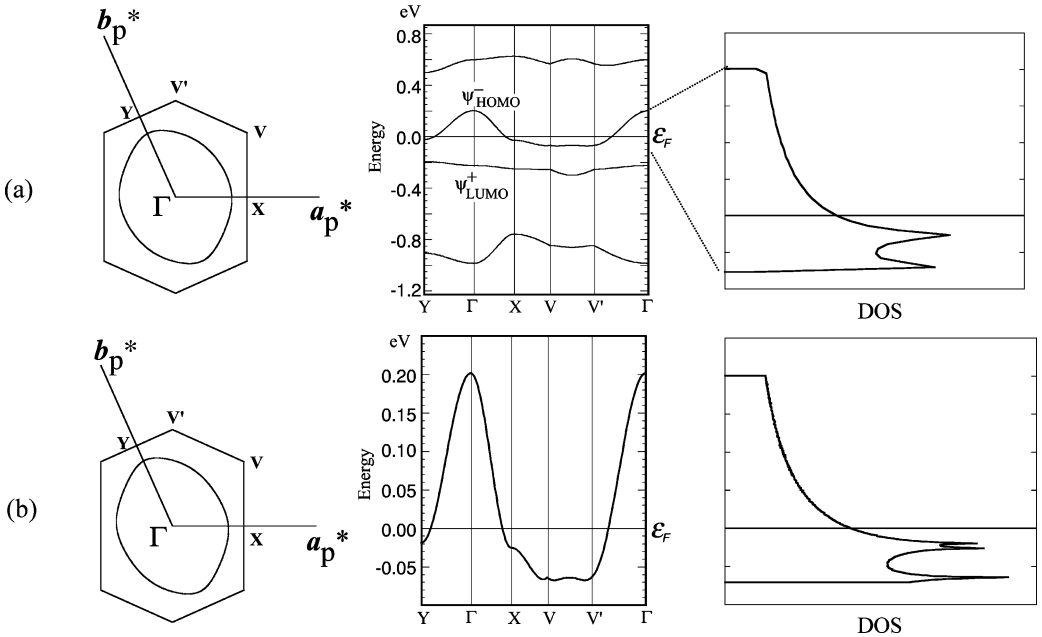

Figure 14. Calculated Fermi surface, band structure, and density of state (DOS) for conduction layer 1 in β'-(Et_2Me_2-As)[Pd(dmit)$_2$]$_2$ at room temperature: (a) calculation including the HOMO and LUMO; (b) calculation based on the dimer model (see text). The C-centered monoclinic cell is reduced to the primitive one as $a_p = (a + b)/2$, $b_p = b$, $c_p = c$.

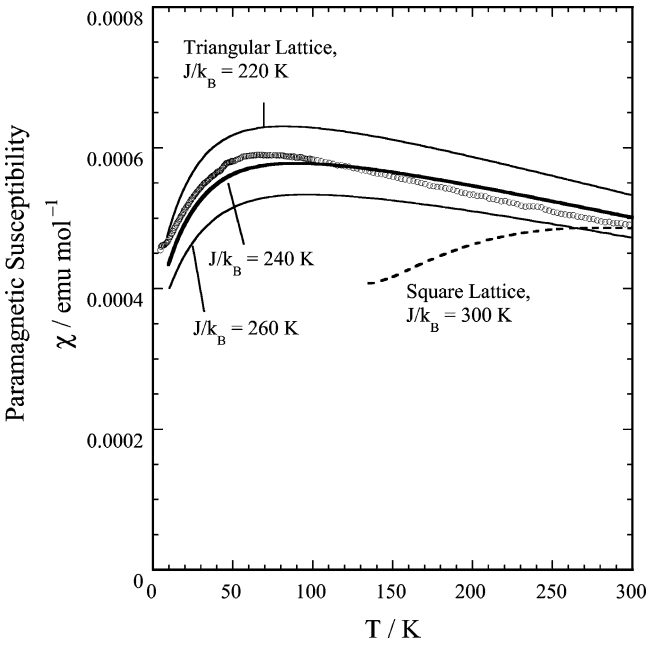

Figure 15. Temperature dependence of static magnetic susceptibility χ for β'-$(Et_2Me_2Sb)[Pd(dmit)_2]_2$. Solid curves show χ calculated for the 2D spin-$^1/_2$ Heisenberg triangular antiferromagnet with various exchange couplings, J. The broken curve denotes χ for the square lattice. (Reprinted with permission from ref 26. Copyright 2002 IOP Publishing Ltd.)

$t_B \approx t_s$) and the uniform 1D chain ($t_r = t_B \rightarrow 0$). Rich physics is expected to lie among these three models. In the present salts, there occurs a crossover where the frustration is released to afford exponential growth of the antiferromagnetic correlation due to the square-lattice-like anisotropy.[135] This explains the decrease of χ in the low-temperature region, followed by the long-range ordering at T_N in the presence of the weak interlayer coupling. The degree of the frustration can be tuned by the choice of the cation and the application of pressure, which plays an important role in determining transport properties under pressure (vide infra).

3.3. Quasi-Three-Dimensional Interaction

The unique feature of the dmit ligand is the terminal thione groups which jut out toward the long molecular axis direction and enable an intermolecular interaction between conduction layers. A precursory example is α-$(Et_2Me_2N)[Ni(dmit)_2]_2$ discussed in section 3.2.1. This compound is characterized by the very short intermolecular S···S contact (3.352 Å) observed between the terminal thione groups as well as by the spanning overlap. An interlayer interaction is roughly estimated to be about $^1/_{10}$ of the intralayer interactions by the calculation of the intermolecular overlap integrals of the LUMOs. The tight-binding calculation indicates that the conduction band has a small but definite dispersion along the third direction (the a^*-axis direction), which was the first case in molecular conductors (Figure 9). The electrical conductivity within the bc plane is isotropic and 20−100 S cm^{-1} at room temperature. It is notable that the conductivity along the a^* axis (interlayer conductivity) is fairly high (1 S cm^{-1} at room temperature).

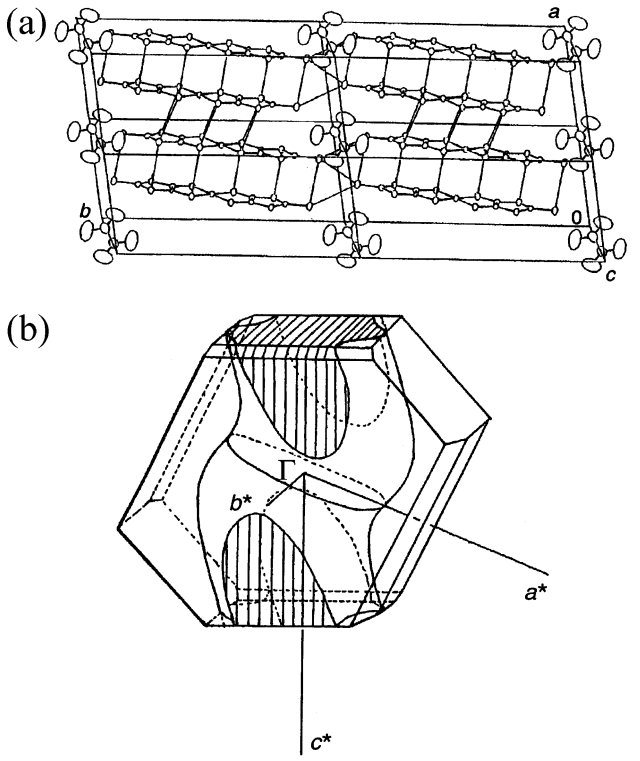

Figure 16. Crystal structure (a) and calculated Fermi surface (b) of $(NHMe_3)[Ni(dmise)_2]_2$. (Reprinted with permission from ref 101. Copyright 1995 Royal Society of Chemistry.)

$M(dmise)_2$ (dmise = 4,5-dimercapto-1,3-dithiole-2-selone) is one of Se-analogues of $M(dmit)_2$, where the terminal thione groups are replaced by selone groups. The larger spatial extension of Se orbitals is expected to enhance the interlayer interaction. The first anion radical salts of $M(dmise)_2$ are α- and β-$(Me_4N)[Ni(dmise)_2]_2$.[103] In the crystal of α-$(Me_4N)[Ni(dmise)_2]_2$, an extremely short intermolecular Se···Se contact (3.277 Å) is observed between the terminal selone groups. Calculated intermolecular overlap integrals of the LUMOs, however, indicate that the interlayer interaction is very weak and α-$(Me_4N)[Ni(dmise)_2]_2$ has quasi-1D electronic structure. This is because the $\pi-\pi$ overlap integral is sensitive not only to the interorbital distance but also to the mutual orbital orientations.

To reduce the layer···layer separation, smaller countercations $NH_{4-x}Me_x^+$ (x = 1, 2, 3) have been examined.[102] Although there is no short interlayer Se···Se contact in $(NH_3Me)[Ni(dmise)_2]_2$ with the smallest cation, $(NHMe_3)[Ni(dmise)_2]_2$ and $(NH_2Me_2)[Ni(dmise)_2]_2$ exhibit enhanced interlayer interactions. $(NHMe_3)[Ni(dmise)_2]_2$ and $(NH_2Me_2)[Ni(dmise)_2]_2$ are isostructural to the corresponding $Ni(dmit)_2$ salts, respectively. In each salt, the triclinic unit cell contains two $Ni(dmise)_2$ anions, and the $Ni(dmise)_2$ anions stack to form a twofold columnar structure (Figure 16). The short interlayer Se···Se distances are 3.801 and 3.486 Å in the $NHMe_3$ salt and 3.504 and 3.617 Å in the NH_2Me_2 salt. Although these Se···Se distances are longer than those in α-$(Me_4N)[Ni(dmise)_2]_2$, both the $NHMe_3$ and NH_2Me_2 salts exhibit large values of interlayer LUMO···LUMO overlap integrals (about 4.5 times larger than that in α-$(Et_2$-

$Me_2N)[Ni(dmit)_2]_2$). Especially in the $NHMe_3$ salt, the interlayer interaction is comparable to the transverse interaction. The tight-binding band calculations based on the LUMO indicate that both salts have 3D electronic structures (Figure 16). Around room temperature, the $NHMe_3$ salt is weakly metallic, while the NH_2Me_2 salt shows almost constant resistivity. Both salts, however, are insulating at low temperature. This would be partially due to the low crystal quality and the positional disorder at the cation sites.

4. Pressure Effect

4.1. Pressure-Induced Metallic and Superconducting States

The electronic states of the molecular conductors can be quite sensitive to the pressure (including *chemical* pressure) application if they are situated near the phase boundary and are soft enough to allow appreciable changes of molecular arrangement and orientation. A typical example is the metal−insulator transition induced by application of a very low hydrostatic pressure (about 100 bar) or deuterium substitution (as chemical pressure) in $(DMe\text{-}DCNQI)_2Cu$.[5] This transition is considered the Mott transition coupled with the Peierls transition. The applied pressure is thought to affect the coordination geometry around the Cu cation and regulate the degree of charge transfer from Cu to DCNQI. The application of hydrostatic pressure has played significant roles in changing the electronic states of low-dimensional molecular conductors, as was demonstrated in the pressure-induced superconductivity of $(TMTSF)_2PF_6$ and its family.[3] In this case, the applied pressure enhances the intercolumn interactions between frontier orbitals and thus the dimensionality of the electronic structure so as to suppress the Peierls instability. This is the most frequently observed pressure effect. Furthermore, development of the uniaxial stress and strain methods has enabled selective or anisotropic regulation of the intermolecular interaction and has provided a powerful means to search for novel electronic states.[136]

As for the molecular conductors based on the metal dithiolene complexes, the number of stable metals at ambient pressure is still limited and the application of pressure plays a crucial role in obtaining the metallic or superconducting states. $Cs_{0.83}[Pd(mnt)_2]\cdot 0.5H_2O$ has an unusual crystal structure among the series of $M(mnt)_2$ salts (Figure 17a).[38] In the crystal, the $Pd(mnt)_2$ anions are strongly dimerized with the eclipsed configuration. The intradimer Pd···Pd distance is 3.329 Å. These dimers form into a 2D array. At ambient pressure, this nonstoichiometric Cs salt exhibits a high conductivity (~5 S cm^{-1} at room temperature) with an activated temperature dependence. With lowering temperature, the system undergoes two semiconductor−semiconductor transitions, one of which is presumably due to the ordering of the Cs^+ ions. Under hydrostatic pressure, transition temperatures for both transitions increase, but activation energies for all phases decrease. Under 18 kbar, the system becomes a stable metal with its resistance still decreasing at 1.2 K (Figure 17b).

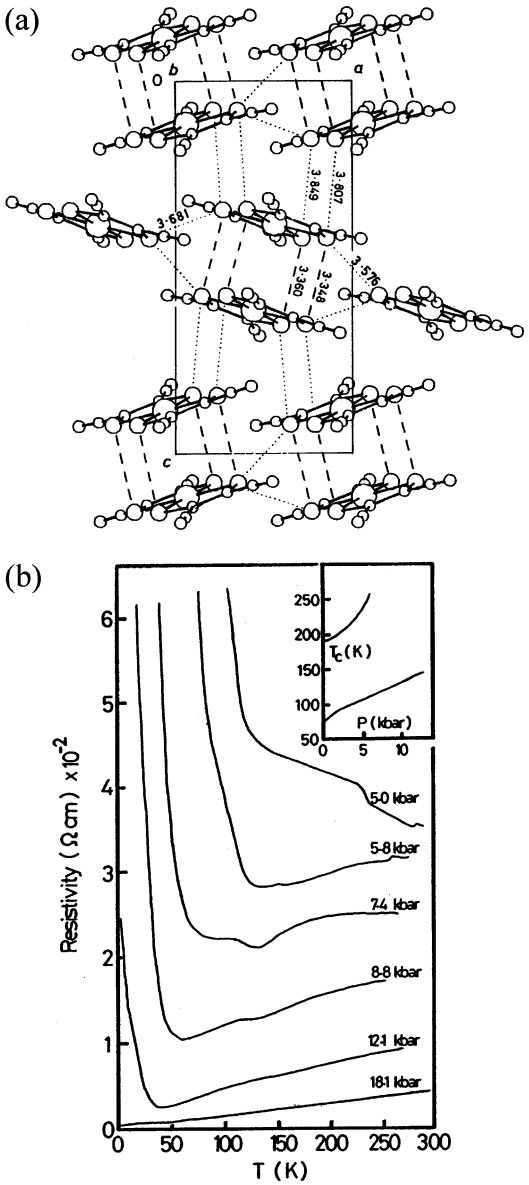

Figure 17. Crystal structure (a) and temperature-dependent resistivity under pressure (b) of $Cs_{0.83}[Pd(mnt)_2]\cdot 0.5H_2O$. (Reprinted with permission from ref 38b,c. Copyright 1989 Royal Society of Chemistry. Copyright 1989 Elsevier Sequoia.)

Unfortunately, details of the electronic structure of this salt were not reported, and the origin of the pressure-induced metallic state remains an open question.

The first molecular superconductor based on the metal dithiolene complex $(TTF)[Ni(dmit)_2]_2$ is a high-pressure superconductor.[12,48] As mentioned in section 3.1.1, this compound belongs to the multisheet Fermi surface system. At ambient pressure, the system remains (semi)metallic with a weak resistivity minimum at 1.5 or 3 K, despite the CDW formation. The system is not superconducting above 47 mK. The application of hydrostatic pressure induces successive phase transitions from the (semi)metallic ground state to semiconducting and reentrant superconducting ground states. In contrast to the cases of the conventional molecular superconductors, the superconducting transition temperature increases slowly with increasing pressure. It is suggested that the

superconductivity coexists with the high-temperature CDW instability and is in weak competition with low-temperature CDW fluctuations. In this multisheet Fermi surface system, these CDWs are considered to affect different parts of the Fermi surface. On the other hand, the Pd-analogue (TTF)[Pd(dmit)$_2$]$_2$ exhibits an insulating ground state due to the CDW formation at ambient pressure.[15,16,48b,80] The application of pressure suppresses the CDW instability and induces the superconductivity with higher transition temperature and higher critical pressure.

At present, every molecular superconductor based on the metal dithiolene complex is derived from the M(dmit)$_2$ (M = Ni, Pd) molecules and is a high-pressure superconductor except for α-(EDT-TTF)[Ni(dmit)$_2$]. The pressure effect has been systematically studied on (Me$_4$Z)[Pd(dmit)$_2$]$_2$ and (Et$_2$Me$_2$Z)[Pd(dmit)$_2$]$_2$ (Z = N, P, As, Sb). Especially, the β' type salts (Z = P, As, Sb) demonstrate the pressure effect on the strongly correlated 2D system with the quasi-triangular lattice.[131] They are Mott insulators at ambient pressure and exhibit various electronic properties including superconductivity under hydrostatic pressure. An important point is that this pressure effect strongly depends on the countercation despite the isostructural molecular packing. The β' type salts can be classified into three types. Type A salts (Me$_4$Z; Z = P, As) remain nonmetallic up to about 17 kbar. Type B salts (Me$_4$Z; Z = Sb. Et$_2$Me$_2$Z; Z = P) show a metallic state accompanied by the superconductivity, and another nonmetallic behavior is observed in the higher pressure region. Type C salts (Et$_2$Me$_2$Z; Z = As, Sb) also turn metallic under hydrostatic pressure, but the superconductivity and the high-pressure nonmetallic behavior are absent.

4.2. Pressure Effect on Crystal and Electronic Structures

To understand the role of pressure, an essential point to discuss is what happens in the molecular arrangement under pressure. β'-(Et$_2$Me$_2$P)[Pd(dmit)$_2$]$_2$ is suitable for this purpose. Figure 18 shows the pressure and temperature dependence of the electronic state of this type B salt.[19,85c,86] Crystal structure analyses were performed under five conditions (Figure 18): APRT (at 293 K and under 1 bar), HPRT1 (at 293 K and under 7.2 kbar), HPLT1 (at 19.1 K and under 7.2 kbar), HPRT2 (at 293 K and under 16.8 kbar), and HPLT2 (at 17.8 K under 20.5 kbar).[137] The unit cell retains the monoclinic symmetry with the space group $C2/c$ under pressure except for at HPLT2. The unit cell of the HPLT2 crystal situated in the high-pressure nonmetallic state is triclinic with the space group $P\bar{1}$. This symmetry breaking is associated with the loss of the glide plane and the twofold axis.

With applying pressure, the interplanar distances decrease more effectively between the dimers than within the dimer. This indicates that the dimer unit is stiff, while the space between the dimers is comparatively flexible. The dimer unit, however, allows a small but significant reduction of the interplanar distance under pressure, which results in a large enhancement of intradimer interactions. Since

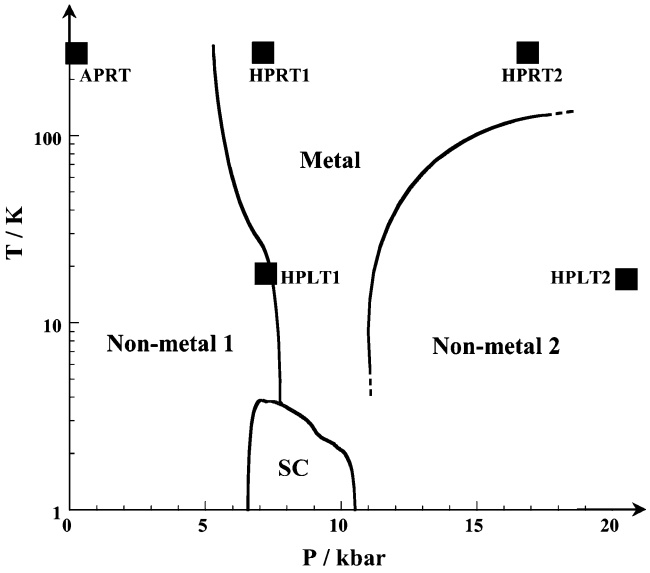

Figure 18. Pressure and temperature dependence of the electronic state for β'-(Et$_2$Me$_2$P)[Pd(dmit)$_2$]$_2$. SC denotes a superconducting state. Inserted marks indicate measurement points for high-pressure structure analyses (see text).

the conduction band of the present system originates mainly from the HOMO of the monomer, we now focus our attention on the intermolecular HOMO···HOMO interactions. Figure 19 shows a pressure dependence of the HOMO···HOMO overlap integrals at room temperature. All these intermolecular interactions are enhanced by increasing pressure. Among them, the intradimer interaction A increases most rapidly. This leads to an *enhancement of the dimerization under pressure*. The situation is the same for the LUMO···LUMO interactions. As mentioned in section 3.2.2, the dimerization gap δ grows with the enhancement of the dimerization. On the other hand, the bandwidth of the conduction band (W) also increases with applying pressure, which can be related to the enhancement of the intermolecular interactions (B, p, q). Formerly, it was proposed that an overlap of the antibonding HOMO band ψ^-_{HOMO} and the bonding LUMO band ψ^+_{LUMO} due to the enhanced bandwidths of the ψ^-_{HOMO} and ψ^+_{LUMO} bands under pressure would lead the system to the metallic state.[85b] This HOMO−LUMO band overlap is expected to remove the half-filled state of the ψ^-_{HOMO} band and induce the metallic state. However, the tight-binding band calculations indicate that the expected HOMO−LUMO band overlap does not occur on every examined condition. This is because the growth of the dimerization gaps overwhelms the increase of the bandwidths.

The intradimer transfer integral t_A is correlated to the effective on-site Coulomb energy on the dimer U_{eff} (see section 3.2.3). Consequently, we can discuss the electron correlation parameter using the ratio t_A/W. It should be noted that U_{eff} as well as W is changeable under pressure, and their competition is a newly identified feature in the strongly correlated system with the dimer structure. At APRT, the system is a Mott insulator with the value $t_A/W = 1.77$. With increasing pressure, the t_A/W value decreases steadily and reaches 1.40 at HPLT1, where the system is situated near the metallic state. This indicates that

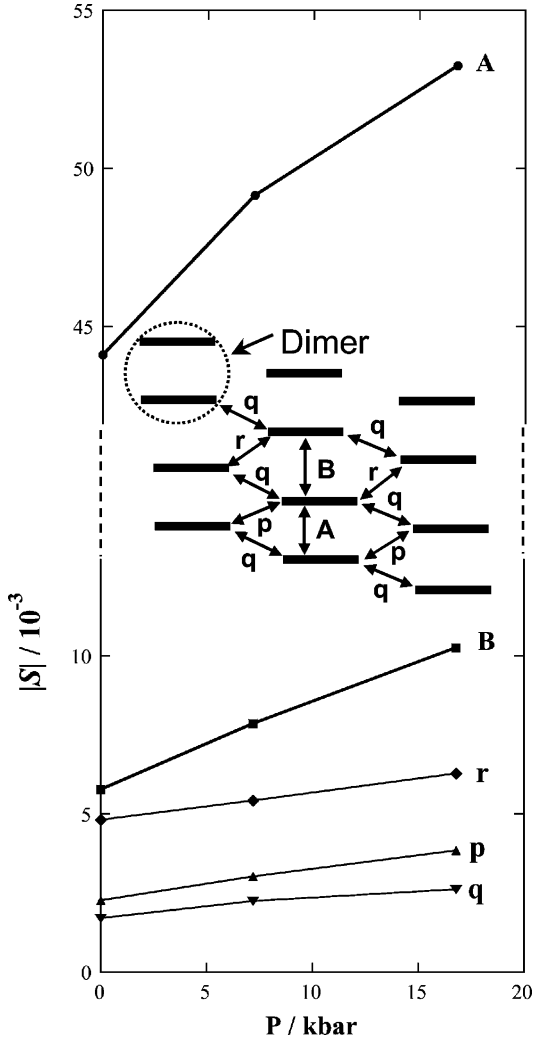

Figure 19. Pressure dependence of HOMO···HOMO overlap integrals (S) at room temperature for β'-(Et_2Me_2P)-$[Pd(dmit)_2]_2$.

the insulator-to-metal transition under pressure is the Mott transition due to the reduced electron correlation. It should be added that the anisotropy of the electronic structure is enhanced with increasing pressure, which is related to the ratio of the intermolecular interaction $|r|/|B|$. In the low-pressure region, ^{13}C NMR measurement revealed that the Néel temperature T_N rises with increasing pressure.[138] This is consistent with the enhanced deviation from the regular triangular lattice under pressure.

As for the high-pressure nonmetallic behavior, the symmetry breaking plays a crucial role. At HPLT2, where the system is in the high-pressure nonmetallic state, the space group symmetry is lowered to $P\bar{1}$, which makes the two conduction layers crystallographically nonequivalent. This allows two conduction bands associated with layers 1 and 2 to have different degrees of anisotropy and filling. The calculated Fermi surface contains a rather anisotropic part (Figure 20). Consequently, it is plausible that the partial nesting of the Fermi surface induces the high-pressure nonmetallic state. It should be noticed that the existence of the nonequivalent conduction layers as well as the HOMO−LUMO band overlap can remove the half-filled state and induce the metallic state. This internal charge transfer between

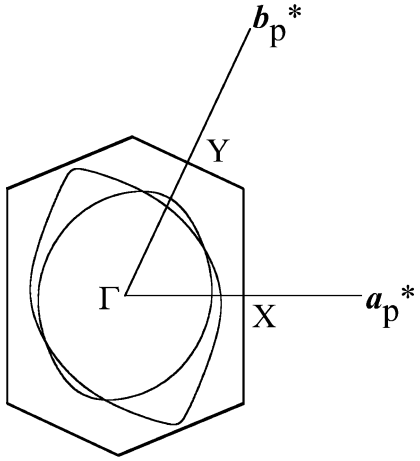

Figure 20. Calculated Fermi surface for β'-$(Et_2Me_2P)[Pd(dmit)_2]_2$ at 17.8 K under 20.5 kbar (at HPLT2 in Figure 18). The C-centered monoclinic cell is reduced to the primitive one as $a_p = (a - b)/2$, $b_p = b$, $c_p = c$.

nonequivalent conduction layers is a kind of "self-doping". At the same time, however, the nonequivalence of the two conduction layers is able to provide the anisotropic Fermi surface which undergoes the (partial) nesting and leads the system to the nonmetallic state.

4.3. Interplay of Correlation and Frustration

The cation dependence observed in the pressure effect indicates that in addition to the electron correlation there is another important factor which governs the electronic state of the β' type $Pd(dmit)_2$ salts. The t_A/W value corresponding to the correlation parameter increases with the cation in the order $Me_4P < Me_4As < Et_2Me_2P \approx Me_4Sb \approx Et_2Me_2As < Et_2Me_2Sb$ (type A < type B < type C; see section 4.1) for the room-temperature structures. The ease of stabilizing the metallic state with (hydrostatic) pressure, however, varies in the same order. Since the metallic state under (hydrostatic) pressure is due to the reduction of the t_A/W value, this looks paradoxical. An important clue is that the Néel temperature T_N at ambient pressure varies with the cation in the reversed order ($Me_4P > Me_4As > Et_2Me_2P \approx Me_4Sb \approx Et_2Me_2As > Et_2Me_2Sb$; Table 8).[133] This order is related to the deviation from the regular triangular lattice t'/t, where $t' = t_r$ and $t = t_B \approx t_s$.[85c] The fact that the Néel temperature T_N is correlated to the stabilization of the metallic state under pressure suggests an important role of the spin frustration.

We now return to the dimer model of the present system (section 3.2.3). The frustration can destroy the long-range spin ordering in the insulating phase. Several theoretical works treat frustration effects in the strongly correlated system and suggest that the metallic phase appears in the region with weaker correlation and stronger frustration.[28] To obtain a general picture, two parameters, t_A/W and t'/t (≤ 1), can be adopted. The former corresponds to the electron correlation parameter, and the latter expresses the frustration parameter. Figure 21 shows a very schematic phase diagram for the present system based on the room-temperature structures. The hydrostatic pressure effect on the Et_2Me_2P salt

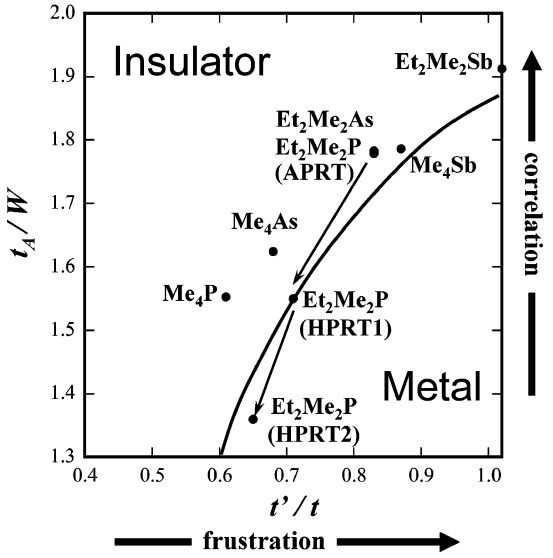

Figure 21. Schematic phase diagram for β'-(cation)[Pd(dmit)$_2$]$_2$ based on the room-temperature structures. The hydrostatic pressure effect for the Et_2Me_2P salt is indicated by arrows. (See also Table 8.)

is indicated by arrows, which illustrate that the application of pressure decreases both t_A/W and t'/t.

4.4. Uniaxial Strain Effect

The uniaxial strain can change only the lattice parameter parallel to the direction of pressure application and regulate the intermolecular interaction selectively. Within the dimer model for the β' type Pd(dmit)$_2$ salts, the electronic state is determined by the intra- and interdimer interactions t_A, t_B, t_s, and t_r, each of which has its own role (see section 3.2.3). Selective regulation of these interactions with the uniaxial strain was first demonstrated for β'-(Me$_4$As)[Pd(dmit)$_2$]$_2$.[21] This compound belongs to type A, and its nonmetallic behavior cannot be suppressed by the application of hydrostatic pressure up to 17.3 kbar. The *b*-axis strain, however, easily suppresses the nonmetallic behavior and induces superconductivity with $T_c = 4$ K at 7 kbar (Figure 22a). On the other hand, the uniaxial strains along the *a*-axis direction *enhance a nonmetallic behavior* in the lower pressure region and a conducting behavior in the higher pressure region (Figure 22b). The low-temperature insulating state cannot be removed by the *a*-axis strain up to 15 kbar. Such a pressure effect is different from those under the hydrostatic pressure and under the *b*-axis strain.

This system has two crystallographically equivalent types of conduction layers, but they are different in the stacking direction of the dimers within each layer (figure in Table 8). In general, the uniaxial strain affects each layer differently except for special directions. One of the special directions is along the *a* axis. The *a* axis is orthogonal to the *b* axis, and thus, the uniaxial strain along this direction should have a small effect on the interdimer interaction t_s. Since the normals of the Pd(dmit)$_2$ molecular planes are at rather small angles (±30°) to the *a* axis, the *a*-axis strain would enhance the interdimer interaction t_B, which affects the bandwidth. At the same time, however, the intradimer interaction t_A would also be enhanced by the *a*-axis strain. This means an increase of the effective on-site Coulomb energy on the dimer (U_{eff}). Therefore, the unique resistivity behavior under the *a*-axis strain can be understood in terms of the competition between U_{eff} and W. The enhancement of the nonmetallic behavior indicates that the increase of U_{eff} overwhelms the increase of W in the low-pressure region.

The *b*-axis strain also gives an equivalent effect on layers 1 and 2. For both conduction layers, the *b*-axis strain is expected to enhance mainly the interdimer interaction t_s, which closely correlates to the bandwidth W, while the intradimer interaction t_A should be less affected. This would effectively reduce the correlation parameter, which induces the metallic behavior.

The uniaxial strain effect also depends on the choice of the cation.[131] The Me$_4$P salt belongs to type A. In contrast to the case of the Me$_4$As salt, the *b*-axis

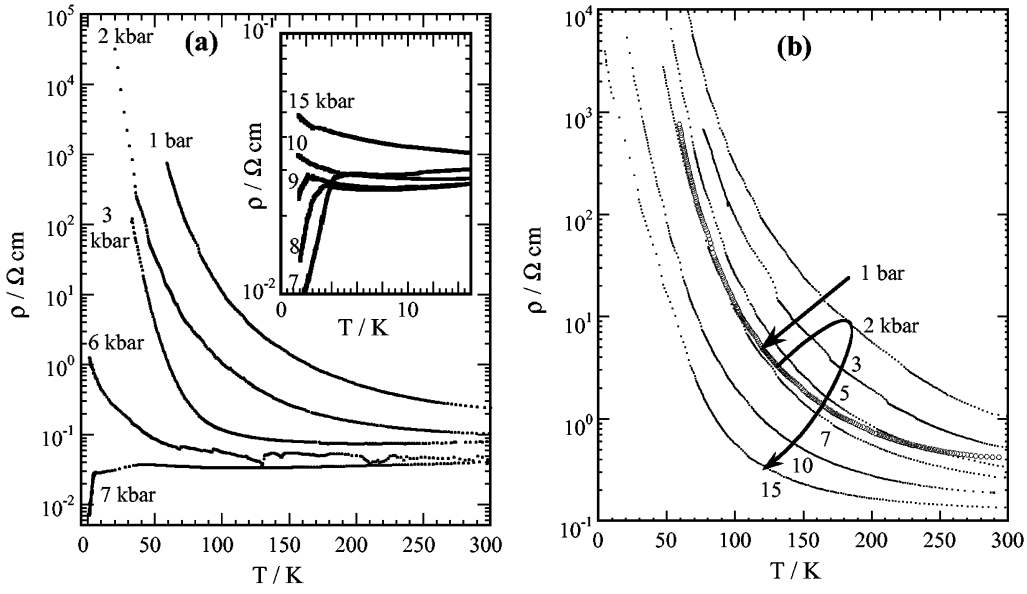

Figure 22. Uniaxial strain effects on resistivity for β'-(Me$_4$As)[Pd(dmit)$_2$]$_2$: (a) *b*-axis strain; (b) *a*-axis strain.

strain cannot suppress the low-temperature insulating state up to 15 kbar. Under the *a*-axis strain, the Me_4P salt shows resistivity behavior similar to that of the Me_4As salt. As for the type B salts, the *b*-axis strain induces the metallic state more effectively than the hydrostatic pressure. For the Et_2Me_2P salt which shows superconductivity at 4 K under the hydrostatic pressure of 7.0 kbar, the *b*-axis strain induces superconductivity at 6.1 K under 4.5 kbar. That is, the *b*-axis strain leads to higher T_c and lower critical pressure. The situation is the same for another type B salt, the Me_4Sb salt, where the resistivity measurement detects superconductivity at 3 K under the hydrostatic pressure of 10 kbar. Under the *b*-axis strain of 4.5 kbar, the Me_4Sb salt exhibits superconductivity at 8.4 K. This is the highest T_c in the molecular superconductors based on the metal dithiolene complexes. On the other hand, the *a*-axis strain effectively enhances the nonmetallic behavior in the low-pressure region for both salts.

5. Supramolecular Cation Effect

The closed-shell counterions in the molecular conductors discussed in this review do not form the conduction band. However, they are not mere spectators, but their size, shape, and charge often have a significant influence on crystal structures and thus physical properties. In this sense, the conducting molecular crystal is *a stage where every man must play a part*. From the viewpoint of the strong correlation between the molecular arrangement and physical properties, introduction of the supramolecular interaction is very useful for crystal engineering.

Introduction of strong and directional supramolecular interactions between the carbon-bound iodine atoms and various species which can act as a Lewis base has been found to be effective in the regulation of molecular arrangement and orientation in conducting cation radical salts.[139] In the anion radical salts of $M(dmit)_2$, the intermolecular chalcogen··· chalcogen contact between the Te-containing cation and the dmit ligand was reported to improve conducting properties. Te atom has a strong tendency to form intermolecular interactions called "secondary bonds" in crystalline compounds.[140]

The crystal structure of $(Me_3Te)[Ni(dmit)_2]_2$ is shown in Figure 23a.[70] This compound exhibits the solid crossing column structure, where the $Ni(dmit)_2$ anions stack along the $a + c$ direction in layer I and along the *a* direction in layer II. In contrast to the case of $(Me_4N)[Ni(dmit)_2]_2$, the crystal belongs to the triclinic system with the space group $P\bar{1}$ and thus these two columns are crystallographically independent and differ from each other in stacking mode. The prominent feature of this salt is the existence of three short Te···S contacts (3.66 and 3.78 Å) between the cation and the terminal thione group in the $Ni(dmit)_2$ anion (Figure 23b). These Te···S contacts are rather shorter than the sum of the van der Waals radii (3.90 Å) and affect the packing of the $Ni(dmit)_2$ anions. Within layer II, especially, the Te atom bridges adjacent $Ni(dmit)_2$ anions aligned along the $a + c$ direction and enhanced the associated intermolecular LUMO···LUMO interaction. This Te atom additionally contacts one terminal thione S atom of the $Ni(dmit)_2$ anion in layer I. The calculated electronic band structure and Fermi surface are shown in Figure 23c. The two conduction bands associated with the crystallographically independent layers differ from each other in dispersion, degree of filling, and Fermi surface. The intermolecular overlap integrals indicate weak dimerization in layer II, which reduces the dimerization gap and leads to an effectively larger bandwidth. The difference in the molecular packing between layers I and II results in the drastic difference in the associated Fermi surfaces. Both Fermi surfaces are strongly warped and indicate a large deviation from the 1D nature. This compound shows clearly metallic behavior down to about 65 K followed by a weak upturn of the resistivity at ambient pressure.

The Te-containing cations have an ability to induce novel arrangements of the $Ni(dmit)_2$ units through the intermolecular Te···S contacts.[70] In β-$(MeTeC_4H_8O)[Ni(dmit)_2]_2$, the 1D supramolecular array of the $MeTeC_4H_8O$ (1-oxa-4-methyl-4-telluracyclohexane) cations through the short Te···O contact (3.33 Å) promotes the herringbone arrangement of the $Ni(dmit)_2$ anions. In addition, short Te···S contacts (3.81 and 3.82 Å) mediate the interlayer S···S contact. This system has a multisheet Fermi surface and exhibits temperature-independent resistivity ($\rho_{RT} = 0.1$ Ωcm) down to about 50 K followed by a moderate upturn.

In the $Pd(dmit)_2$ system, the trialkyltelluronium cations with the trigonal pyramidal geometry also exhibit Te···S interactions, which play a significant role in determining the molecular arrangement and thus electronic structure. $(Me_3Te)[Pd(dmit)_2]_2$ has the solid crossing column structure with two crystallographically nonequivalent conduction layers (I and II, Figure 24).[91] Notably, the Me_3Te cations contact only layer I with short Te···S distances (3.50 and 3.65 Å). This geometrical difference in the cation···anion contacts between layers I and II causes different overlap modes of the $Pd(dmit)_2$ anions. Consequently, the two energy bands associated with conduction layers I and II are clearly different in dispersion, degree of filling, and shape of the Fermi surface (Figure 24c). As discussed in section 4.2, the existence of the nonequivalent conduction layers can remove the half-filled state and induce the metallic state. Indeed, the Me_3Te salt clearly shows metallic behavior down to about 50 K without applying pressure. Below this temperature, an upturn of the resistivity occurs. The system, however, remains moderately conductive even at 4.2 K, which suggests that this compound has conduction electrons even at the lowest temperature. An origin of the transition around 50 K is thought to be the partial nesting of the Fermi surface.

The Te···S interaction is also observed in $(Et_2MeTe)[Pd(dmit)_2]_2$, but in a different manner.[91,92] The crystal belongs to the triclinic system with the space group $P\bar{1}$ and consists of two crystallographically independent conduction layers (I and II, Figure 25). In contrast to the case of the Me_3Te salt, the $Pd(dmit)_2$ columns are parallel to the *a*-axis direction within both layers. The Et_2MeTe cation contacts two

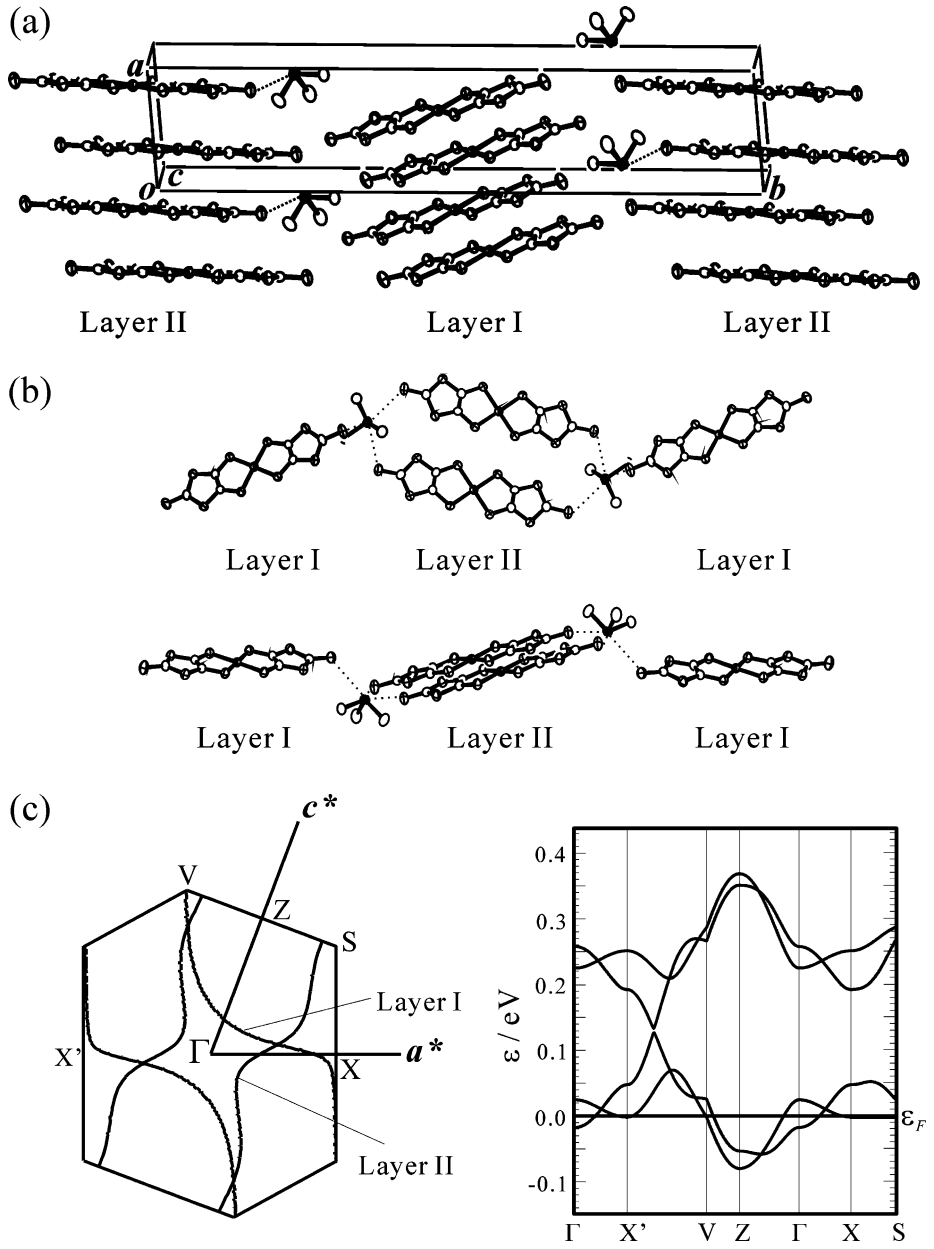

Figure 23. Crystal structure (a), intermolecular Te···S contacts (b), and band structure (c) for $(Me_3Te)[Ni(dmit)_2]_2$. (Reprinted with permission from ref 70. Copyright 2002 Royal Society of Chemistry.)

$Pd(dmit)_2$ molecules in the dimer within layer I, whereas it contacts only one $Pd(dmit)_2$ molecule within layer II. In addition, the Et_2MeTe cation mediates the interlayer S···S interaction and leads to the sizable interlayer overlap integral. In layer I, the cations squeeze into the dimer through short Te···S contacts and behave as *props*. Competition between strong Pd···Pd and Te···S contacts bends the outer five-membered ring toward the terminal thione groups in adjacent dimers. In the HOMO of $Pd(dmit)_2$, the thione S atom p orbitals are out of phase with other S atom p orbitals (Figure 1). These features reduce the interdimer HOMO···HOMO interaction within the column and make the overall interdimer interaction more isotropic. Therefore, the calculated Fermi surface associated with layer I is closed, whereas the one for layer II is open. The Et_2MeTe salt shows a metallic behavior down to 30−40 K. Below this temperature, an upturn of the resistivity occurs. The system, however, remains moderately conductive even at 4.2 K.

The above examples demonstrate that the Te-based secondary bond can be used for the tuning of the molecular arrangement and thus intermolecular interactions in the anion radical salts.

Another type of supramolecular structure has been studied in the conducting $Ni(dmit)_2$ salts with crown ether macrocycles.[6h] The crown ethers accommodate alkali metal ions forming supramolecular cation structures. Three kinds of crown ethers (12-crown-4, 15-crown-5, and 18-crown-6) and an acyclic polyether (pentaethyleneglycol) were examined.

The crown ethers can form an ion channel which provides for transport of Li^+ cations.[141] In the crystal of $Li_{0.6}(15\text{-crown-}5)H_2O[Ni(dmit)_2]_2$, the crown ether macrocycles uniformly stack to form a 1D ion channel structure (Figure 26). The Li cations are observed just above and just below the center of gravity of the

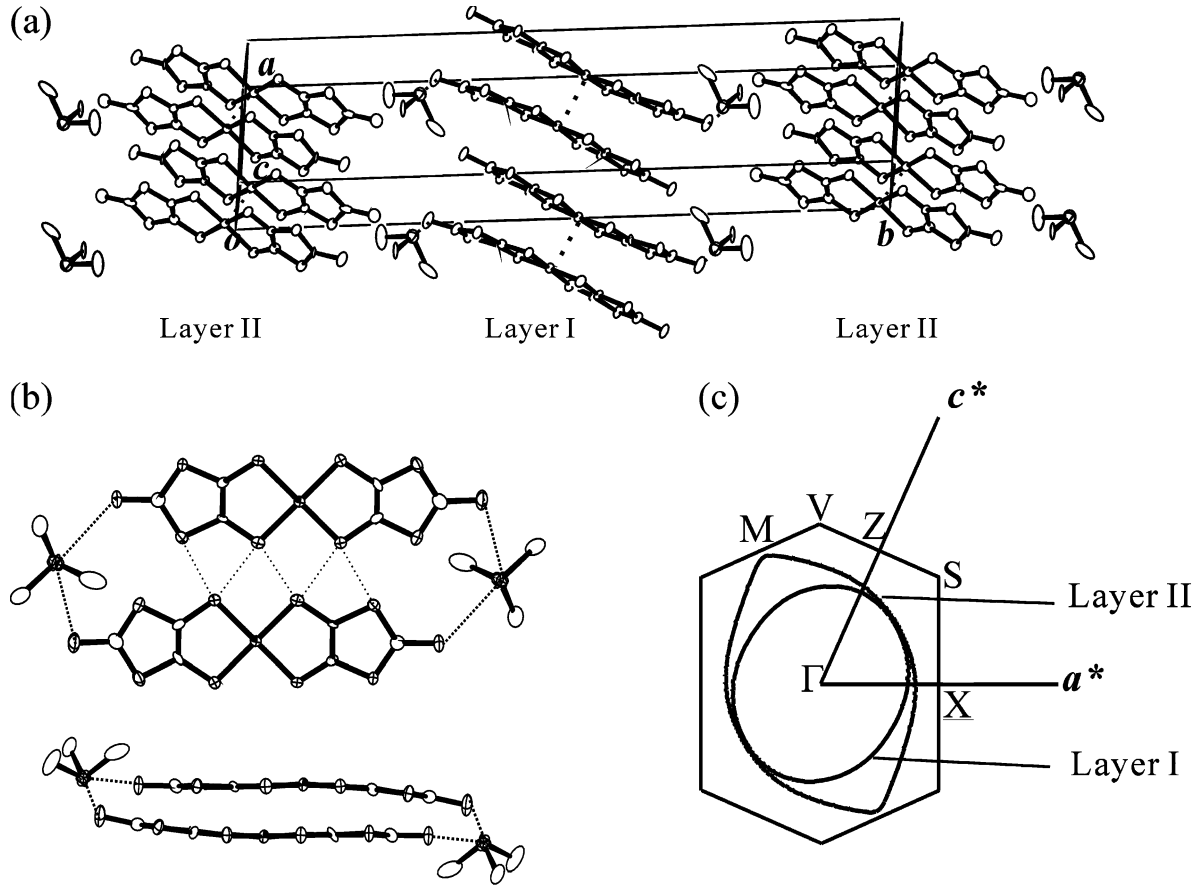

Figure 24. Crystal structure (a), intermolecular Te···S contacts within layer I (b), and calculated Fermi surface (c) for $(Me_3Te)[Pd(dmit)_2]_2$.

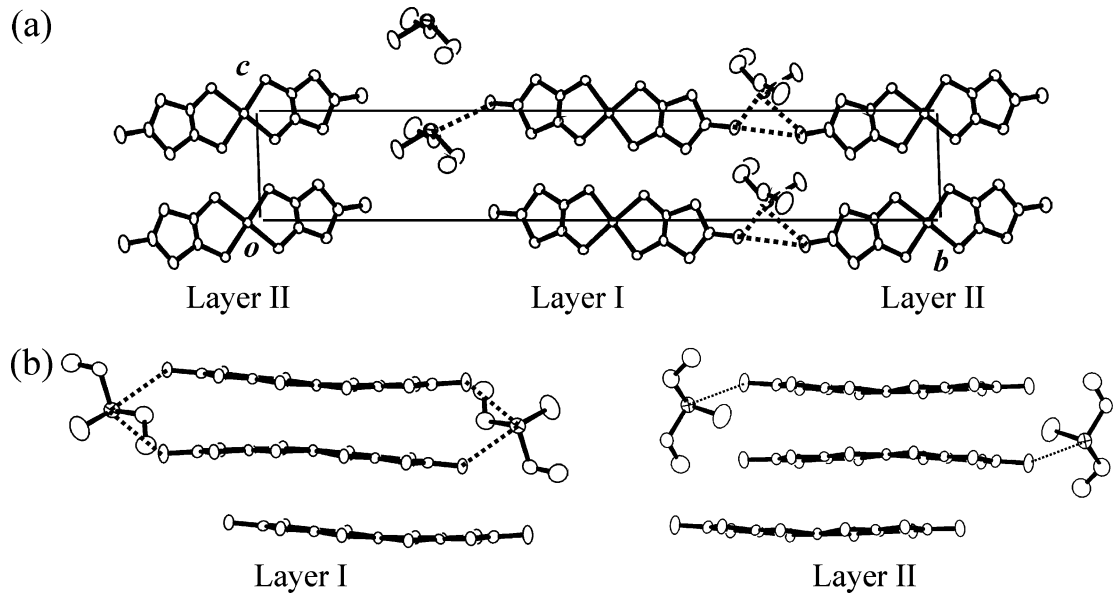

Figure 25. Crystal structure (a) and intermolecular Te···S contacts (b) for $(Et_2MeTe)[Pd(dmit)_2]_2$.

crown ether molecule with the occupancy factor of 0.3, while one water molecule is located at the midpoint of two neighboring crown ether molecules. The $Ni(dmit)_2$ anions form a uniform 1D column parallel to the supramolecular cation column. The pairs of the $Ni(dmit)_2$ columns are separated from each other by the supramolecular cation column, which prevents the formation of short S···S contacts between the adjacent pairs. This salt shows high room-temperature conductivity (about 240 S cm^{-1}) and a crossover from a metallic state near room temperature to a magnetic insulator state below about 200 K. This crossover is attributed to the interaction between the Li^+ cations in the channels and the electrons in the $Ni(dmit)_2$ columns. In the low-temperature region, the Li^+ cations form random potentials which pin the conduction electrons in the $Ni(dmit)_2$ columns. In the high-temperature region, however, the Li^+ cations are mobile in the channel and they no longer form random potentials which

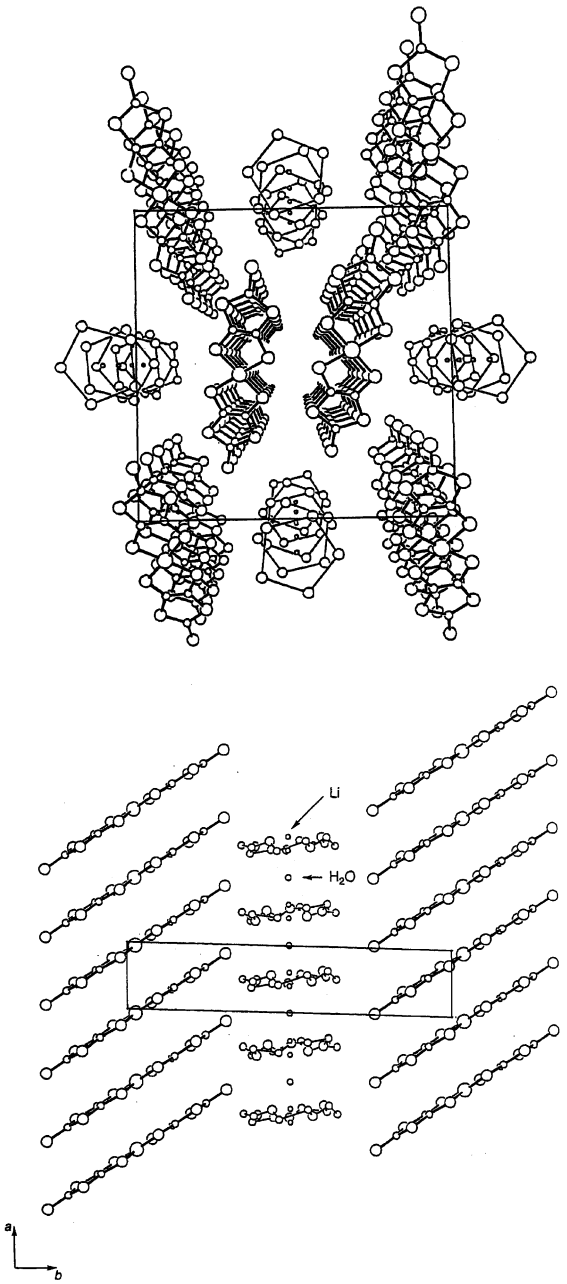

Figure 26. Crystal structure of $Li_{0.6}$(15-crown-5)H_2O[Ni(dmit)$_2$]$_2$. (Reprinted with permission from ref 141. Copyright 1998 Macmillan Publisher Ltd.)

localize the conduction electrons. Indeed, the ^{7}Li NMR and ion cunductivity measurements indicate that the Li^+ cations in the crystal are mobile above 250 K and become immobilized between 250 and 200 K. It should be added that since the cation sites are not completely occupied, the band-filling control with tuning of the Li^+ content would be possible in this type of materials.

6. Conclusion

Metal dithiolene complexes have provided a number of unique molecular conductors and will remain the vast frontier of highly functionalized molecular systems. The two-MO picture—the interplay of the HOMO and LUMO—associated with the small HOMO−LUMO level splitting is an essential and fascinating part of the electronic structure. The single-component molecular metal is one of the landmarks which the two-MO nature has generated. Such an orbital degree of freedom is a newly identified aspect of the molecular conductor. The unique crystal architectures including the solid crossing column structure, the spanning overlap mode, and the strong dimerization have opened new routes toward molecular materials with high performance. Molecular conductors based on the metal dithiolene complexes embrace rich physics concerning the Peierls instability of the low-dimensional system, the strong correlation, the charge separation, the frustration, and so on. The application of pressure has played a crucial role in studying these physical properties. Technical progress in physical measurements under high pressure, coupled with the first-principles band calculation for the high-pressure condition,[142] will bring about much more information and reveal the uncharted nature of this fascinating class of materials. On the other hand, the application of supramolecular chemistry is one of the key approaches to highly functionalized materials which operate even at ambient pressure.

7. Note Added in Proof

During publication of this review, we found that a sufficiently pure crystal of β'-(Et_2Me_2As)[Pd(dmit)$_2$]$_2$ exhibited superconductivity at 5.5 K under 8 kbar. Although this salt is classified into type C in Table 8, this new result suggests that the Et_2Me_2As salt would belong to type B, which is consistent with the t_A/W vs t'/t mapping in Figure 21.

8. References

(1) Kagoshima, S.; Kato, R.; Fukuyama, H.; Seo, H.; Kino, H. In *Advances in Synthetic Metals—Twenty Years of Progress in Science and Technology*; Bernier, P., Lefrant, S., Bidan, G., Eds.; Elsevier: 1999; p 262.

(2) Kagoshima, S.; Nagasawa, H.; Sambongi, T. *One-Dimensional Conductors*; Springer series in solid-state science Vol. 72; Springer-Verlag: Berlin, 1988.

(3) (a) Bechgaard, K.; Jacobsen, C. S.; Mortensen, K.; Pedersen, H. J.; Thorup, N. *Solid State Commun*. **1980**, *33*, 1119. (b) Jérome, D.; Mazaud, A.; Ribault, M.; Bechgaard, K. *J. Phys. Lett*. **1980**, *41*, L95. (c) As a review see for example: Ishiguro, T.; Yamaji, K.; Saito, G. *Organic Superconductors*; Springer: 1998.

(4) Williams, J. M.; Ferraro, J. R.; Thorn, R. J.; Carlson, K. D.; Geiser, U.; Wang, H. H.; Kini, A. M.; Whangbo, M.-H. *Organic Superconductors (Including Fullerenes)*; Prentice Hall: Englewood Cliffs, NJ, 1992.

(5) Kato, R. *Bull. Chem. Soc. Jpn*. **2000**, *73*, 515.

(6) (a) Clemenson, P. I. P. *Coord. Chem. Rev*. **1990**, *106*, 171. (b) Cassoux, P.; Valade, L.; Kobayashi, H.; Kobayashi, A.; Clark, R. A.; Underhill, A. E. *Coord. Chem. Rev*. **1991**, *110*, 115. (c) Cassoux, P.; Valade, L. In *Inorganic Materials*; Bruce, D. W., O'Hare, D., Eds.; Wiley: 1997; Chapter 1. (d) Kobayashi, A.; Kobayashi, H. In *Handbook of Organic Conductive Molecules and Polymers*; Nalwa, H. S., Ed.; John Wiley & Sons Ltd: 1997; Vol. 1, p 249. (e) Canadell, E. *New. J. Chem*. **1997**, *21*, 1147. (f) Cassoux, P. *Coord. Chem. Rev*. **1999**, *186*, 213. (g) Canadell, E. *Coord. Chem. Rev*. **1999**, *185−186*, 629. (h) Nakamura, T.; Akutagawa, T. *Coord. Chem. Rev*. **2000**, *198*, 297. (i) Robertson, N.; Cronin, L. *Coord. Chem. Rev*. **2002**, *227*, 93. (j) Pullen, A. E.; Olk, R.-M. *Coord. Chem. Rev*. **1999**, *188*, 211.

(7) Kato, R.; Kashimura Y.; Sawa, H.; Okano, Y. *Chem. Lett*. **1997**, 921.

(8) (a) Miller, J. S.; Epstein, A. J. *Prog. Inorg. Chem*. **1976**, *20*, 1. (b) Underhill, A. E.; Watkins, D. M. *Chem. Soc. Rev*. **1980**, *9*, 429. (c) Williams, J. M.; Schultz, A. J.; Underhill, A. E.; Carneiro, K. In *Extended Linear Chain Compounds*; Miller, J. S., Ed.; Plenum: New York, 1982; Vol. 1, p 73.

(9) Underhill, A. E.; Ahmad, M. M. *J. Chem. Soc., Chem. Commun*. **1981**, 67.
(10) Valade, L.; Bousseau, M.; Gleizes, A.; Cassoux, P. *J. Chem. Soc., Chem. Commun*. **1983**, 110.
(11) Kato, R.; Kobayashi, H.; Kim, H.; Kobayashi, A.; Sasaki, Y.; Mori, T.; Inokuchi, H. *Chem. Lett*. **1988**, 865.
(12) Brossard, L.; Ribault, M.; Bousseau, M.; Valade, L.; Cassoux, P. *C. R. Acad. Sci., Ser. II* **1986**, *302*, 205.
(13) Kobayashi, A.; Kim, H.; Sasaki, Y.; Kato, R.; Kobayashi, H.; Moriyama, S.; Nishio, Y.; Kajita, K.; Sasaki, W. *Chem. Lett*. **1987**, 1819.
(14) Tajima, H.; Inokuchi, M.; Kobayashi, A.; Ohta, T.; Kato, R.; Kobayashi, H.; Kuroda, H. *Chem. Lett*. **1993**, 1235.
(15) Brossard, L.; Hurdequint, H.; Ribault, M.; Valade, L.; Legros, L.-P.; Cassoux, P. *Synth. Met*. **1988**, *27*, B157.
(16) Brossard, L.; Ribault, M.; Valade, L.; Cassoux, P. *J. Phys. (Paris)* **1989**, *50*, 1521.
(17) Kobayashi, A.; Kobayashi, H.; Miyamoto, A.; Kato, R.; Clark, R. A.; Underhill, A. E. *Chem. Lett*. **1991**, 2163.
(18) Kobayashi, H.; Bun, K.; Naito, T.; Kato, R.; Kobayashi, A. *Chem. Lett*. **1992**, 1909.
(19) Kato, R.; Kashimura, Y.; Aonuma, S.; Hanasaki, N.; Tajima, H. *Solid State Commun*. **1998**, *105*, 561.
(20) (a) Kashimura, Y. Doctor Thesis, The University of Tokyo, 1998. (b) Eguchi, A.; Tamura, M.; Nishio, Y.; Kajita, K. Unpublished.
(21) Kato, R.; Tajima, N.; Tamura, M.; Yamaura, J.-I. *Phys. Rev. B* **2002**, *66*, 020508.
(22) Canadell, E.; Rachidi, I. E.-I.; Ravy, S.; Pouget, J.-P.; Brossard, L.; Legros, J.-P. *J. Phys. (Paris)* **1989**, *50*, 2967.
(23) Kato, R.; Yamamoto, K.; Kashimura, Y.; Okano, Y.; Aonuma, S. *Synth. Met*. **1999**, *103*, 2020.
(24) Kanoda, K. *Hyperfine Interact.* **1997**, *104*, 235.
(25) Collins, M. F.; Petrenko, O. A. *Can. J. Phys*. **1997**, *75*, 605.
(26) Tamura, M.; Kato, R. *J. Phys.: Condens. Matter* **2002**, *14*, L729.
(27) Kino, H.; Fukuyama, H. *J. Phys. Soc. Jpn*. **1996**, *65*, 2158.
(28) (a) Kondo, H.; Moriya, T. *J. Phys. Soc. Jpn.* **1999**, *68,* 3170. (b) Morita, H.; Watanabe S.; Imada, M. *J. Phys. Soc. Jpn*. **2002**, *71*, 2109.
(29) Almeida, M.; Henriques, R. T. In *Handbook of Organic Conductive Molecules and Polymers*; Nalwa, H. S., Ed.; John Wiley & Sons Ltd: 1997; Vol. 1, p 87.
(30) Kato, R.; Imakubo, T.; Yamamoto, H.; Maeda, R.; Fujiwara, M.; Yamaura, J.-I.; Sawa, H. *Mol. Cryst. Liq. Cryst*. **2002**, *380*, 61.
(31) (a) Gama, V.; Henriques, R. T.; Almeida, M.; Alcácer, L. *J. Phys. Chem*. **1994**, *98*, 997. (b) Gama, V.; Almeida, M.; Henriques, R. T.; Santos, I. C.; Domingos, A.; Ravy, S.; Pouget, J. P. *J. Phys. Chem*. **1991**, *95*, 4263.
(32) (a) Alcácer, L.; Morgado, J.; Henriques, R. T.; Almeida, M. *Synth. Met*. **1995**, *70*, 1093. (b) Morgado, J.; Santos, I. C.; Veiros, L. F.; Henriques, R. T.; Duarte, M. T.; Almeida, M.; Alcácer, L. *J. Mater. Chem*. **1997**, *7*, 2387.
(33) (a) Ribera, E.; Rovira, C.; Veciana, J.; Tarres, J.; Canadell, E.; Rousseau, R.; Molins, E.; Mas, M.; Schoeffel, J. P.; Pouget, J. P.; Morgado, J.; Henriques, R. T.; Almeida, M. *Chem. Eur. J*. **1999**, *5*, 2025. (b) Ribera, E.; Rovira, C.; Veciana, J.; Tarres, J.; Canadell, E.; Rousseau, R.; Molins, E.; Mas, M.; Schoeffel, J. P.; Pouget, J. P.; Morgado, J.; Gama, V.; Henriques, R. T.; Almeida, M. *Synth. Met*. **1999**, *102*, 1743.
(34) Reith, W.; Polborn, K.; Amberger, E. *Angew. Chem., Int. Ed. Engl*. **1988**, *27*, 699.
(35) Nishijo, J.; Ogura, E.; Yamaura, J.; Miyazaki, A.; Enoki, T.; Takano, T.; Kuwatani, Y.; Iyoda, M. *Solid State Commun*. **2000**, *116*, 661.
(36) (a) Henriques, R. T.; Alcácer, L. A.; Pouget, J. P.; Jérome, D. *J. Phys. C: Solid State Phys*. **1984**, *17*, 5197. (b) Henriques, R. T.; Alcácer, L. A.; Jérome, D.; Bourbonnais, C.; Weyl, C. *J. Phys. C: Solid State Phys*. **1986**, *19*, 4663. (c) Domingos, A.; Henriques, R. T.; Gama, V.; Almeida, M.; Vieira, A. L.; Alcácer, L. *Synth. Met*. **1988**, *27*, B411.
(37) Batsanov, A. S.; Moore, A. J.; Robertson, N.; Green, A.; Bryce, M. R.; Howard, J. A. K.; Underhill, A. E. *J. Mater. Chem*. **1997**, *7*, 387.
(38) (a) Parker, I. D.; Friend, R. H.; Clemenson, P. I.; Underhill, A. E. *Nature* **1986**, *324*, 547. (b) Hursthouse, M. B.; Short, R. L.; Clemenson, P. I.; Underhill, A. E. *J. Chem. Soc., Dalton Trans*. **1989**, 1101. (c) Parker, I. D.; Friend, R. H.; Underhill, A. E. *Synth. Met.* **1989**, *29*, F195.
(39) (a) Kobayashi, A.; Sasaki, Y.; Kobayashi, H.; Underhill, A. E.; Ahmad, M. M. *J. Chem. Soc., Chem. Commun*. **1982**, 390. (b) Kobayashi, A.; Mori, T.; Sasaki, Y.; Kobayashi, H.; Ahmad, M. M.; Underhill, A. E. *Bull. Chem. Soc. Jpn*. **1984**, *57*, 3262.
(40) Kobayashi, A.; Sasaki, Y.; Kobayashi, H. *Chem. Lett*. **1984**, 305.
(41) Ahmad, M. M.; Turner, D. J.; Underhill, A. E.; Kobayashi, A.; Sasaki, Y.; Kobayashi, H. *J. Chem. Soc., Dalton Trans*. **1984**, 1759.
(42) Arcon, D.; Lappas, A.; Margadonna, S.; Prassides, K.; Ribera, E.; Veciana, J.; Rovira, C.; Henriques, R. T.; Almeida, M. *Phys. Rev. B* **1999**, *60*, 4191.
(43) Tarres, J.; Mas, M.; Molins, E.; Veciana, J.; Rovira, C.; Morgado, J.; Henriques, R. T.; Almeida, M. *J. Mater. Chem*. **1995**, *5*, 1653.
(44) Uruichi, M.; Yakushi, K.; Yamashita, Y.; Qin, J. *J. Mater. Chem*. **1998**, *8*, 141.
(45) Gama, V.; Henriques, R. T.; Bonfaint, G.; Pereira, L. C.; Waerenborgh, J. C.; Santos, I. C.; Duarte, M. T.; Cabral, J. M. P.; Almeida, M. *Inorg. Chem.* **1992**, *31*, 2598.
(46) (a) Gama, V.; Henriques, R. T.; Bonfaint, G.; Almeida, M.; Meetsma, A.; van Smaalen, S.; de Boer, J. L. *J. Am. Chem. Soc.* **1992**, *114*, 1986. (b) Veiros, L. F.; Calhorda, M. J.; Canadell, E. *Inorg. Chem.* **1994**, *33*, 4290.
(47) Gama, V.; Henriques, R. T.; Almeida, M.; Veiros, L.; Calhorda, M. J.; Meetsma, A.; de Boer, J. L. *Inorg. Chem.* **1993**, *32*, 3705.
(48) (a) Bousseau, M.; Valade, L.; Legros, J.-P.; Cassoux, P.; Garbauskas, M.; Interrante, L. V. *J. Am. Chem. Soc*. **1986**, *108*, 1908. (b) Ravy, S.; Pouget, J.-P.; Valade, L.; Legros, J.-P. *Europhys. Lett*. **1989**, *9*, 391. (c) Brossard, L.; Ribault, M.; Valade, L.; Cassoux, P. *Phys. Rev. B* **1990**, *42*, 3935.
(49) Kato, R.; Kobayashi, H.; Kobayashi, A.; Sasaki, Y. *Chem. Lett*. **1985**, 131.
(50) (a) Kato, R.; Kobayashi, H.; Kobayashi, A.; Naito, T.; Tamura, M.; Tajima, H.; Kuroda, H. *Chem. Lett*. **1989**, 1839. (b) Kobayashi, A.; Sato, A.; Kawano, K.; Naito, T.; Kobayashi, H.; Watanabe, T. *J. Mater. Chem*. **1995**, *5*, 1671.
(51) Kobayashi, H.; Kato, R.; Kobayashi, A.; Sasaki, Y. *Chem. Lett*. **1985**, 191.
(52) Kobayashi, A.; Kato, R.; Kobayashi, H.; Mori, T.; Inokuchi, H. *Physica B* **1986**, *143*, 562.
(53) Kobayashi, H.; Kato, R.; Kobayashi, A.; Sasaki, Y. *Chem. Lett*. **1985**, 535.
(54) Jacobsen, C. S.; Yatsev, V. M.; Tanner, D. B.; Bechgaard, K. *Synth. Met*. **1993**, *56*, 1925.
(55) Sawa, H.; Okano, Y.; Aonuma, S.; Kato, R. *Synth. Met*. **1995**, *70*, 1055.
(56) Kato, R.; Aonuma, S.; Okano, Y.; Sawa, H.; Kobayashi, A.; Kobayashi, H. *Synth. Met*. **1993**, *56*, 2084.
(57) (a) Faulmann, C.; Errami, A.; Legros, J.-P.; Cassoux, P.; Yagubskii, E. B.; Kotov, A. I. *Synth. Met*. **1993**, *56*, 2057. (b) Faulmann, C.; Errami, A.; Donnadieu, B.; Malfant, I.; Legros, J.-P.; Cassoux, P.; Rovira, C.; Canadell, E. *Inorg. Chem*. **1996**, *35*, 3856.
(58) Pomarède, B.; Garreau, B.; Malfant, I.; Valade, L.; Cassoux, P.; Legros, J.-P.; Audouard, A.; Brossard, L.; Ulmet, J.-P.; Doublet, M.-L.; Canadell, E. *Inorg. Chem*. **1994**, *33*, 3401.
(59) (a) Kim, H.; Kobayashi, A.; Sasaki, Y.; Kato, R.; Kobayashi, H. *Chem. Lett*. **1987**, 1799. (b) Kajita, K.; Nishio, Y.; Moriyama, S.; Kato, R.; Kobayashi, H.; Sasaki, W.; Kobayashi, A.; Kim, H.; Sasaki, Y. *Solid State Commun.* **1988**, *65*, 361.
(60) (a) Tajima, H.; Ikeda, S.; Inokuchi, M.; Kobayashi, A.; Ohta, T.; Sasaki, T.; Toyota, N.; Kato, R.; Kobayashi, H.; Kuroda, H. *Solid State Commun*. **1993**, *88*, 605. (b) Kobayashi, A.; Naito, T.; Kobayashi, H. *Phys. Rev. B* **1995**, *51*, 3198.
(61) Kato, R.; Kobayashi, H.; Kim, H.; Kobayashi, A.; Sasaki, Y.; Mori, T.; Inokuchi, H. *Synth. Met*. **1988**, *27*, B359.
(62) Kobayashi, A.; Naito, T.; Sato, A.; Kobayashi, H. *Synth. Met*. **1997**, *86*, 1841.
(63) Kato, R.; Mori, T.; Kobayashi, A.; Sasaki, Y.; Kobayashi, H. *Chem. Lett*. **1984**, 1.
(64) Valade, L.; Legros, J.-P.; Bousseau, M.; Cassoux, P.; Garbauskas, M.; Interrante, L. V. *J. Chem. Soc., Dalton Trans*. **1985**, 783.
(65) Kobayashi, H.; Kato, R.; Kobayashi, A. *Synth. Met*. **1991**, *42*, 2495.
(66) Kobayashi, A.; Naito, T.; Sato, A.; Kobayashi, H. *Mol. Cryst. Liq. Cryst*. **1996**, *284*, 85.
(67) Pullen, A. E.; Liu, H.-L.; Tanner, D. B.; Abboud, K. A.; Reynolds, J. R. *J. Mater. Chem*. **1997**, *7*, 377.
(68) (a) Nakamura, T.; Underhill, A. E.; Coomber, A. T.; Friend, R. H.; Tajima, H.; Kobayashi, A.; Kobayashi, H. *Synth. Met*. **1995**, *70*, 1061. (b) Liu, H. L.; Tanner, D. B.; Pullen, A. E.; Abboud, K. A.; Reynolds, J. R. *Phys. Rev. B* **1996**, *53*, 10557.
(69) Valade, L.; Legros, J.-P.; Cassoux, P.; Kubel, F. *Mol. Cryst. Liq. Cryst*. **1986**, *140*, 335.
(70) Fujiwara, M.; Kato, R. *J. Chem. Soc., Dalton Trans*. **2002**, 3763.
(71) (a) Veldhuizen, Y. S. J.; Haasnoot, J. G.; Reedijk, J. *Synth. Met*. **1997**, *86*, 1827. (b) Veldhuizen, Y. S. J.; Smeets, W. J. J.; Veldman, N.; Spek, A. L.; Faulmann, C.; Auban-Senzier, P.; Jérome, D.; Paulus, P. M.; Haasnoot, J. G.; Reedijk, J. *Inorg. Chem*. **1997**, *36*, 4930.
(72) Miyazaki, A.; Izuoka, A.; Sugawara, T. *Bull. Chem. Soc. Jpn*. **1993**, *66*, 2832.
(73) Reefman, D. J.; Cornelissen, J. P.; Haasnoot, J. G.; de Graaf, R. A. G.; Reedijk, J. *Inorg. Chem*. **1990**, *29*, 3933.
(74) Veldhuizen, Y. S. J.; Veldman, N.; Spek, A. L.; Faulmann, C.; Haasnoot, J. G.; Reedijk, J. *Inorg. Chem*. **1995**, *34*, 140.
(75) Cornelissen, J. P.; Muller, E.; Vaassens, P. H. S.; Haasnoot, J. G.; Reedijk, J.; Cassoux, P. *Inorg. Chem*. **1992**, *31*, 2241.
(76) (a) Akutagawa, T.; Nakamura, T.; Inabe, T.; Underhill, A. E. *Thin Solid Films* **1998**, *331*, 264. (b) Akutagawa, T.; Nakamura, T.; Inabe, T.; Underhill, A. E. *J. Mater. Chem.* **1997**, *7*, 183.

(77) Nakamura, T.; Akutagawa, T.; Honda, K.; Underhill, A. E.; Coomber, A. T.; Friend, R. H. *Nature* **1998**, *394*, 161.
(78) Imai, H.; Inabe, T.; Otsuka, T.; Okuno, T.; Awaga, K. *Phys. Rev. B* **1996**, *54*, R6838.
(79) Malfant, I.; Andreu, R.; Lacroix, P. G.; Faulmann, C.; Cassoux, P. *Inorg. Chem*. **1998**, *37*, 3361.
(80) Legros, J.-P.; Valade, L. *Solid State Commun*. **1988**, *68*, 599.
(81) (a) Doublet, M.-L.; Canadell, E.; Garreau, B.; Legros, J.-P.; Brossard, L.; Cassoux, P.; Pouget, J.-P. *J. Phys.: Condens. Matter* **1995**, *7*, 4673. (b) Brossard, L.; Ribaoult, M.; Garreau, B.; Pomarede, B.; Cassoux, P. *Europhys. Lett*. **1992**, *19*, 223.
(82) (a) Imakubo, T.; Sawa, H.; Kato, R. *J. Chem. Soc., Chem. Commun*. **1995**, 1097. (b) Hanasaki, N.; Tajima, H.; Imakubo, T.; Kato, R. *J. Phys. Soc. Jpn*. **2003**, *72*, 2291.
(83) Kobayashi, A.; Kim, H.; Sasaki, Y.; Murata, K.; Kato, R.; Kobayashi, H. *J. Chem. Soc., Faraday Trans*. **1990**, *86*, 361.
(84) Kobayashi, A.; Miyamoto, A.; Kato, R.; Sato, A.; Kobayashi, H. *Bull. Chem. Soc. Jpn*. **1998**, *71*, 997.
(85) (a) Faulmann, C.; Legros, J.-P.; Cassoux, P.; Cornelissen, L.; Brossard, L.; Inokuchi, M.; Tajima, H.; Tokumoto, M. *J. Chem. Soc., Dalton Trans*. **1994**, 249. (b) Kato, R.; Liu, Y.-L.; Hosokoshi, Y.; Aonuma, S.; Sawa, H. *Mol. Cryst. Liq. Cryst*. **1997**, *296*, 217. (c) Rouzière, S.; Yamaura, J.-I.; Kato, R. *Phys. Rev. B* **1999**, *60*, 3113.
(86) Aonuma, S.; Sawa, H.; Kato, R. *Synth. Met*. **1997**, *86*, 1881.
(87) Kramer, G. J.; Jol, J. C.; Brom, H. B.; Groeneveld, L. R.; Reedijk, J. *J. Phys. C: Solid State Phys.* **1988**, *21*, 4591.
(88) Legros, J.-P.; Valade, L.; Cassoux, P. *Synth. Met*. **1988**, *27*, B347.
(89) Kato, R.; Fujiwara, M.; Kashimura, Y.; Yamaura, J. *Synth. Met*. **2001**, *120*, 675.
(90) Faulmann, C.; Doublet, M.-L.; Granier, F.; Garreau de Bonneval, B.; Malfant, I.; Legros, J.-P.; Togonidze, T.; Cassoux, P. *J. Mater. Chem*. **2001**, *11*, 2205.
(91) (a) Kato, R.; Fujiwara, M.; Kashimura, Y.; Yamaura, J. *Synth. Met*. **2001**, *120*, 675. (b) Fujiwara, M. Doctor Thesis, The University of Tokyo, 2001.
(92) Kato, R.; Imakubo, T.; Yamamoto, H.; Maeda, R.; Fujiwara, M.; Yamaura, J.-I.; Sawa, H. *Mol. Cryst. Liq. Cryst*. **2002**, *380*, 61.
(93) Naito, T.; Inabe, T.; Kobayashi, H.; Kobayashi, A. *J. Mater. Chem*. **2001**, *11*, 2199.
(94) Underhill, A. E.; Clark, R. A.; Marsden, I.; Allan, M.; Friend, R.; Tajima, H.; Naito, T.; Tamura, M.; Kuroda, H.; Kobayashi, A.; Kobayashi, H.; Canadell, E.; Ravy, S.; Pouget, J. P. *J. Phys.: Condens. Matter* **1991**, *3*, 933.
(95) Kobayashi, A.; Sasaki, Y.; Kato, R.; Kobayashi, H. *Chem. Lett*. **1986**, 387.
(96) Kobayashi, A.; Miyamoto, A.; Kobayashi, H.; Clark, A.; Underhill, A. E. *J. Mater. Chem*. **1991**, *1*, 827.
(97) Shibaeva, R. P.; Rozenberg, L. P.; Kushch, L. A.; Kotov, A. I.; Khomenko, A. G.; Yagubskii, E. B.; Zavodnik, V. E. *Synth. Met*. **1992**, *46*, 261.
(98) Kotov, A. V.; Kushch, L. A.; Laukhin, N. V.; Khomenko, A. G.; Zvarykina, A. V.; Shibaeva, R. P.; Yagubskii, E. B.; Nagapetyan, S. S.; Struchkov, Yu. T. *Synth. Met*. **1991**, *42*, 2355.
(99) Świetlik, R.; Lapiński, A.; Kushch, L. A.; Yagubskii, E. B. *J. Phys. (Paris)* **1996**, *6*, 1643.
(100) (a) Broderick, W. E.; McGhee, E. M.; Godfrey, M. R.; Hoffman, B. M.; Ibers, J. A. *Inorg. Chem*. **1989**, *28*, 2902. (b) Martin, J. D.; Canadell, E.; Batail, P. *Inorg. Chem*. **1992**, *31*, 3176.
(101) Naito, T.; Sato, A.; Kawano, K.; Tateno, A.; Kobayashi, H.; Kobayashi, A. *J. Chem. Soc., Chem. Commun*. **1995**, 351.
(102) Sato, A.; Kobayashi, H.; Naito, T.; Sakai, F.; Kobayashi, A. *Inorg. Chem*. **1997**, *36*, 5262.
(103) Cornelissen, J. P.; Pomarède, B.; Spek, A. L.; Reefman, D.; Haasnoot, J. G.; Reedijk, J. *Inorg. Chem*. **1993**, *32*, 3720.
(104) Sato, A.; Kobayashi, H.; Kobayashi, A. *Chem. Lett*. **1997**, 1275.
(105) Olk, R.-M.; Kirmse, R.; Hoyer, E.; Faulmann, C.; Cassoux, P. *Z. Anorg. Allg. Chem*. **1994**, *620*, 90.
(106) (a) Shibaeva, R. P.; Zavodnik, V. E. *Kristallografiya* **1993**, *38*, 84. (b) Doublet, M.-L.; Canadell, E.; Pouget, J.-P.; Shibaeva, R. P. *J. Phys. I* **1994**, *4*, 1439.
(107) (a) Yagubskii, E. B.; Kotov, A. I.; Buravov, L. I.; Khomenko, A. G.; Shklover, V. E.; Nagapetyan, S. S.; Struchkov, Yu. T.; Vetoshkina, L. V.; Ukhin, L. Yu. *Synth. Met.* **1990**, *35*, 271. (b) Yagubskii, E. B.; Kotov, A. I.; Laukhina, E. E.; Ignatiev, A. A.; Buravov, L. I.; Khomenko, A. G.; Shklover, V. E.; Nagapetyan, S. S.; Struchkov, Yu. T.; Nesmeyanov, A. N. *Synth. Met.* **1991**, *42*, 2515.
(108) Nagapetyan, S. S.; Shklover, V. E.; Struchkov, Yu. T.; Kotov, A. I.; Yagubskii, E. B.; Ukhin, L. Yu. *Dokl. Akad. Nauk SSSR* **1990**, *310*, 94.
(109) Kushch, L. A.; Gritsenko, V. V.; Buravov, L. I.; Khomenko, A. G.; Shilov, G. V.; Dyachenko, O. A.; Merzhanov, V. A.; Yagubskii, E. B.; Rousseau, R.; Canadell, E. *J. Mater. Chem.* **1995**, *5*, 1633.
(110) Kushch, L. A.; Konovalikhin, S. V.; Buravov, L. I.; Khomenko, A. G.; Shilov, G. V.; Van, K.; Dyachenko, O. A.; Yagubskii, E. B.; Rovira, C.; Canadell, E. *J. Phys. I* **1996**, *6*, 1555.
(111) Yagubskii, E. B.; Kushch, L. A.; Gritsenko, V. V.; Dyachenko, O. A.; Buravov, L. I.; Khomenko, A. G. *Synth. Met.* **1995**, *70*, 1039.
(112) Kushch, L. A.; Yagubskii, E. B.; Konovalikhin, S. V.; Shilov, G. V.; Atovmyan, L. O. *Russ. Chem. Bull*. **1999**, *48*, 1513.
(113) Gritsenko, V. V.; Dyachenko, O. A.; Kushch, L. A.; Yagubskii, E. B. *Synth. Met.* **1998**, *94*, 61.
(114) Dyachenko, O. A.; Gritsenko, V. V.; Shilov, G. V.; Laukhina, E. E.; Yagubskii, E. B. *Synth. Met.* **1993**, *58*, 137.
(115) Watanabe, E.; Fujiwara, M.; Yamaura, J.; Kato, R. *J. Mater. Chem.* **2001**, *11*, 2131.
(116) Miyazaki, T.; Ohno, T. *Phys. Rev. B* **1999**, *59*, R5269.
(117) Tajima, H.; Naito, T.; Tamura, M.; Kobayashi, A.; Kuroda, H.; Kato, R.; Kobayashi, H.; Clark, R. A.; Underhill, A. E. *Solid State Commun*. **1991**, *79*, 337.
(118) Kobayashi, A.; Kim, H.; Sasaki, Y.; Kato, R.; Kobayashi, H. *Solid State Commun*. **1987**, *62*, 57.
(119) Mori, T.; Kobayashi, A.; Sasaki, Y.; Kobayashi, H.; Saito, G.; Inokuchi, H. *Bull. Chem. Soc. Jpn*. **1984**, *57*, 627.
(120) (a) Seo, H. *J. Phys. Soc. Jpn*. **2000**, *69*, 805. (b) Mori, T. *Bull. Chem. Soc. Jpn*. **2000**, *73*, 2243. (c) Mori, T. *J. Phys. Soc. Jpn*. **2003**, *72*, 1469.
(121) Tamura, M.; Kato, R. *Chem. Phys. Lett*. **2004**, *387*, 448.
(122) Ishibashi, S.; Kohyama, M. *Phys. Rev. B* **2000**, *62*, 7839.
(123) Kanai, K.; Shin, S. *RIKEN Rev.* **2002**, *46*, 10.
(124) Kobayashi, A.; Tanaka, H.; Kobayashi, H. *J. Mater. Chem*. **2001**, *11*, 2078.
(125) Tanaka, H.; Okano, Y.; Kobayashi, H.; Suzuki, W.; Kobayashi, A. *Science* **2001**, *291*, 285.
(126) Tajima, H.; Naito, T.; Tamura, M.; Takahashi, A.; Toyoda, S.; Kobayashi, A.; Kuroda, H.; Kato, R.; Kobayashi, H.; Clark, R. A.; Underhill, A. E. *Synth. Met*. **1991**, *41*−*43*, 2417.
(127) Tajima, H.; Inokuchi, M.; Arifuku, M.; Ohta, T.; Kobayashi, A.; Kato, R.; Kobayashi, H. *Synth. Met*. **1995**, *70*, 1035.
(128) Inabe, T. *J. Porphyrins Phthalocyanines* **2001**, *5*, 3.
(129) (a) Rosa, A.; Ricciardi, G.; Baerends, E. J. *Inorg. Chem*. **1998**, *37*, 1368. (b) Alvarez, S.; Vicente, R.; Hoffman, R. *J. Am. Chem. Soc*. **1985**, *107*, 6253.
(130) Doublet, M.-L.; Canadell, E.; Pouget, J. P.; Yagubskii, E. B.; Ren, J.; Whangbo, M.-H. *Solid State Commun*. **1993**, *88*, 699.
(131) (a) Kato, R.; Tajima, A.; Tajima, N.; Nakao, A.; Tamura, M. *J. Phys. IV* **2004**, *114*, 411. (b) Tajima, A.; Nakao, A.; Kato, R. Submitted to *J. Phys. Soc. Jpn*.
(132) Mori, M.; Yonemitsu, K.; Kino, H. *Mol. Cryst. Liq. Cryst*. **2000**, *341*, 549.
(133) Nakamura, T.; Takahashi, T.; Aonuma, S.; Kato, R. *J. Mater. Chem.* **2001**, *11*, 2159.
(134) Recently, we have found that newly synthesized Et_2Me_2Sb salt undergoes a unique charge separation transition which leads to a nonmagnetic insulating state at about 70 K under ambient pressure. It is considered that the local quantum resonance mechanism proposed in ref 121 operates in this charge separation transition. Notably, in the previous sample prepared in the presence of Et_3MeSb^+ ions as impurities, the charge separation transition is completely suppressed. Surprisingly, no anomaly was detected at the cation site in the previous sample by the ordinary X-ray crystal structure analysis.
(135) Tamura, M.; Kato, R. *J. Phys. IV* **2004**, *114*, 383.
(136) Maesato, M.; Kaga, Y.; Kondo, R.; Kagoshima, S. *Rev. Sci. Instrum*. **2000**, *71*, 176.
(137) Yamaura, J.-I.; Nakao, A.; Kato, R. *J. Phys. Soc. Jpn*. **2004**, *73*, 976.
(138) (a) Takano, Y.; Hiraki, K.; Kato, R.; Takahashi, T. *Synth. Met*. **2003**, *135*−*136*, 593. (b) Takano, Y. Doctor Thesis, Gakushuin University, 2003.
(139) (a) Imakubo, T.; Sawa, H.; Kato, R. *Synth. Met.* **1997**, *86*, 1847. (b) Imakubo, T.; Maruyama, T.; Sawa, H.; Kobayashi, K. *Chem. Commun*. **1998**, 2021. (c) Imakubo, T.; Tajima, N.; Tamura, M.; Kato, R.; Nishio, Y.; Kajita, K. *J. Mater. Chem*. **2002**, *12*, 159. (d) Tajima, N.; Imakubo, T.; Kato, R.; Nishio, Y.; Kajita, K. *J. Phys. Soc. Jpn*. **2003**, *72*, 1014. (e) Yamamoto, H. M.; Yamaura, J.; Kato, R. *J. Am. Chem. Soc*. **1998**, *120*, 5905. (f) Yamamoto, H. M.; Maeda, R.; Yamaura, J.; Kato, R. *J. Mater. Chem.* **2001**, *11*, 1034.
(140) (a) Alcock, N. W. *Adv. Inorg. Chem. Radiochem*. **1972**, *15*, 1 (b) Haiduc, I.; King, R. B.; Newton, M. G. *Chem. Rev*. **1994**, *94*, 302. (c) Pyykkö, P.; *Chem. Rev.* **1997**, *97*, 597.
(141) Nakamura, T.; Akutagawa, T.; Honda, K.; Underhill, A. E.; Coomber, T.; Friend, R. H. *Nature* **1998**, *394*, 159.
(142) Miyazaki, T.; Ohno, T. *Phys. Rev. B* **2003**, *68*, 035116.

CR030655T